endo- versus *exo*-Cyclic coordination in copper complexes with methylthiazolylcarboxylate tacn derivatives[i]

Amaury Guillou[a], Luís M. P. Lima[b], David Esteban-Gómez[c], Rita Delgado[b], Carlos Platas-Iglesias[c], Véronique Patinec[a] and Raphaël Tripier[a*]

[a] Université de Bretagne Occidentale, UMR-CNRS 6521, UFR des Sciences et Techniques, 6 avenue Victor le Gorgeu, C.S. 93837, 29238 Brest Cedex 3, France

[b] Instituto de Tecnologia Química e Biológica António Xavier, Universidade Nova de Lisboa, Av. da República, 2780-157 Oeiras, Portugal

[c] Universidade da Coruña, Centro de Investigacións Científicas Avanzadas (CICA) and Departamento de Química, Facultade de Ciencias, 15071, A Coruña, Galicia, Spain

Dalton Transactions, volume 48, issue 24, pages 8740–8755, 28 June 2019
Submitted 30 March 2019, accepted 16 May 2019, first published 17 May 2019

How to cite:

A. Guillou, L. M. P. Lima, D. Esteban-Gómez, R. Delgado, C. Platas-Iglesias, V. Patinec and R. Tripier, *endo*- versus *exo*-Cyclic coordination in copper complexes with methylthiazolylcarboxylate tacn derivatives, *Dalt. Trans.*, 2019, **48**, 8740–8755. DOI: 10.1039/C9DT01366K.

Abstract

Three tacn (1,4,7-triazacyclononane)-based ligands substituted by methylthiazolylcarboxylate (**tha**) and/or methylthiazolyl (**th**) arms have been examined for copper complexation with the aim to study the impact of carboxylate groups on the complexation of Cu(II), which can present an *endo*- or *exo*-cyclic coordination. Two new ligands have been synthesised: H_3**no3tha**, tacn bearing three methylthiazolylcarboxylate arms, and H_2**no1th2tha**, tacn with one methylthiazolyl and two methylthiazolylcarboxylate arms, while H**no2th1tha** had already been described. Their complexation behaviour with 1 or 1.5 equivalents of metal was studied on the basis of preliminary results showing the tendency of **tha** arms to form exocyclic polynuclear species. The solid state studies of the Cu(II) and Zn(II) complexes were investigated and some of their structures were characterised by X-ray diffraction. The physicochemical properties of the complexes in solution were also investigated by means of potentiometric measurements, UV-vis spectroscopy, EPR and computational studies, NMR characterisation of the corresponding Zn(II) complexes and redox behaviour by electrochemistry. Mono- and tri-nuclear complexes ML and M_3L_2 were formed and isolated, highlighting the tendency of methylthiazolylcarboxylate arms, when carried by a tacn platform, to form *exo*-cyclic and polynuclear complexes. However, this exhaustive study evidences that the "out of cage" and "in cage" present different behaviour in terms of stability.

Introduction

The coordination chemistry of copper cations is involved in many applications and processes in various domains linked to biology and medicine. A few examples among the many that could be cited are

* raphael.tripier@univ-brest.fr

Alzheimer's disease, in which copper and other ions are located in amyloid-β peptide aggregates,[1] the active sites of enzymes like multicopper oxydase,[2] and the use of copper complexes as therapeutic agents[3] or in diagnostic imaging, employing the copper-64 radioisotope for positron emission tomography (PET).[4] Copper complexes proved to be relevant for modelling the cupric cation activity in biological systems,[1,2] and precious for developing new bioconjugates for imaging and therapy.[3,4] The coordination environment in copper(ii) complexes is often accomplished by N and/or O donor atoms because of the borderline acid nature of this cation according to Pearson's classification of hard and soft acids and bases (HSAB).[5] New elaborated acyclic and cyclic polydentate chelating systems like functionalised Schiff bases and polyamines have been developed for efficient coordination of this metal ion.[6,7] Studies for characterising the resulting copper chelates under conditions similar to those of biological medium remain essential for understanding the evolving nature of the copper(ii) complexes in these media. The characterisation of cupric complexes generally involves the description of structures in the solid state and in solution by using suitable diffractometric and spectroscopic methods, as well as access to thermodynamic and kinetic data. The redox behaviour of the Cu(i)/Cu(ii) system often constitutes a central point for mimicking the active sites of enzymes, but it also remains necessary for medical applications because of the possible reduction of the metal ion by enzymes or bioreductors present *in vivo* giving rise to the dissociation of the resulting more labile Cu(i) chelate.[8]

The 1,4,7-triazacyclononane (tacn) scaffold is one of the macrocyclic polyamine platforms that has been widely used in these research areas for Cu(ii) complexation, often by varying the nature and number of coordinating pendant arms, which may contain for instance acetate,[9] pyridine,[10] imidazol,[11] phenolate,[12] or picolinate[13] groups. Because of the small size of the macrocyclic cavity compared to other azamacrocycles like cyclam, the metal ion is placed above the mean plane of the macrocycle coordinated to the nitrogen atoms of amine functions. Additional donor atoms from pendant arms could complete the coordination sphere giving rise to penta- or hexa-coordinated complexes,[9–14] with the metal lodged inside the formed cage. However, polynuclear edifices may be formed when the macrocycle does not present any *N*-appended function, with the metal coordination environment being completed by the presence of co-ligands, solvent molecules, or counterions.[15] The "in-cage" endocyclic coordination is maintained in architectures containing two or three tacn units linked by aromatic cores, producing di- or tri-nuclear metal complexes, in which a metal cation as copper can be bridged by phosphinate groups,[16] hydroxyde,[17] acetate,[18] phosphate,[19] chloride,[20] or oxalate[21] anions. Polynuclear structures may also be promoted by the presence of additional donor atoms in the pendant arms, so that one or more *N*-added arms link one or more macrocycles by coordinating an "out-of-cage" exocyclic metal.[22]

We recently described copper(ii) complexes of tacn substituted by two (**no2th**) or three (**no3th**) methylthiazolyl arms exhibiting CuN_5 distorted square pyramidal and CuN_6 distorted trigonal prismatic "in-cage" geometries, respectively (Scheme 1).[23,24] The modification of the **no3th** ligand by adding an acetate function on the alpha position of the N atom of one of the thiazolyl groups (H**no2th1tha**) was also investigated.[24] The physico-chemical properties of the [Cu(**no2th1tha**)]$^+$ complex were found to be very close to those of [Cu(**no2th**)]$^{2+}$ and [Cu(**no3th**)]$^{2+}$ complexes in terms of thermodynamic stability and kinetic inertness. The crystals of [Cu(**no2th1tha**)]$^+$, obtained under acidic conditions, revealed a CuN_4Cl coordination sphere provided by the three nitrogen atoms of the macrocycle, one nitrogen atom of one methylthiazolyl arm and a chloride anion, resulting in a distorted square pyramidal geometry. A protonated methylthiazolyl arm and the methylthiazolylcarboxylate pendant arm were not involved in the coordination of the copper(ii) centre. More interestingly, the relatively stable Cu_3L_2 species (L = ligand) was identified by potentiometry whenever a 1.5 : 1 Cu(ii)/L ratio was used. The formation of Cu_3L_2 species was justified by a potential "out-of-cage" coordination of one of the metal ions by two methylthiazolylcarboxylate arms of different ligand moieties.

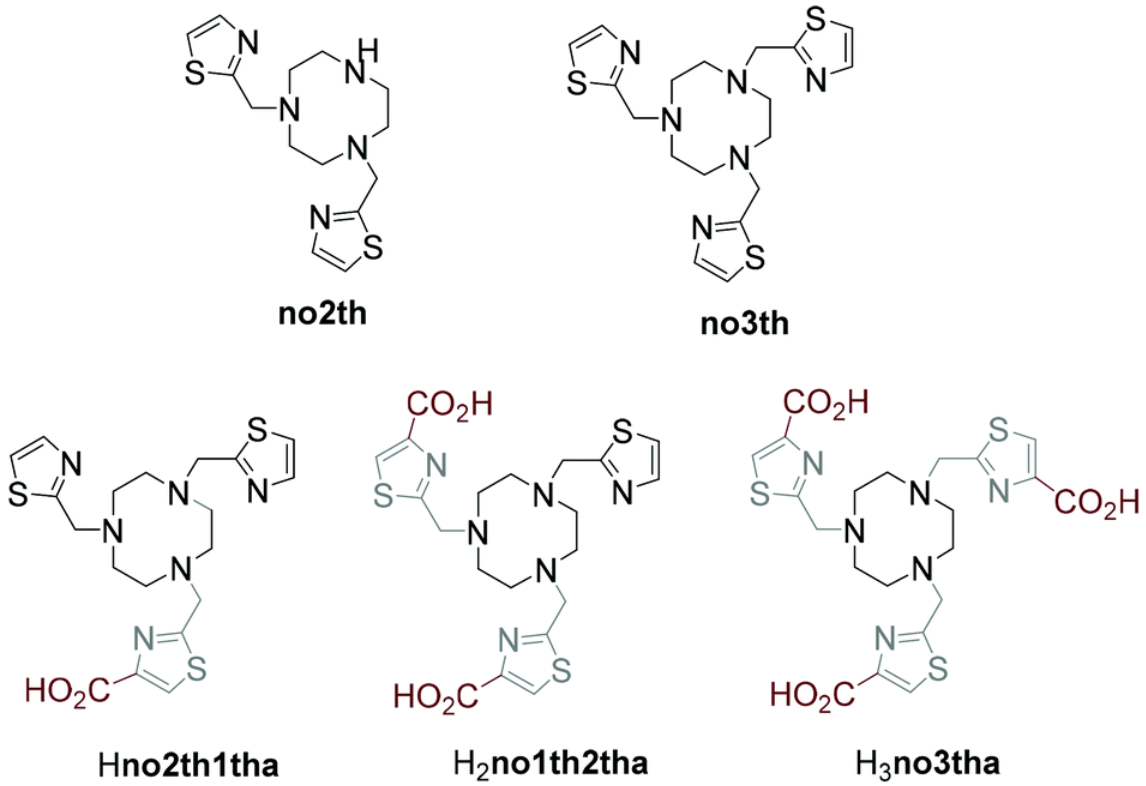

Scheme 1. Ligands discussed in this study.

Considering the interesting behaviour of the H**no2th1tha** ligand, we were curious to understand the impact that incorporating two or three methylthiazolylcarboxylate pendant arms on the tacn moiety has on the physico-chemical properties of the corresponding copper complexes and the generation of "in-cage" or "out-of-cage" structures. Thus, in the current work, we present the synthesis of the two new triaza polyfunctionalised ligands H_2**no1th2tha** and H_3**no3tha** (Scheme 1) and compare their coordination properties with those of H**no2th1tha** and **no2th**. We provide structural evidence for the formation of Cu_3L_2 species through the "out-of-cage" coordination of a metal ion. We report a detailed analysis of the thermodynamic stability and electrochemical properties of the complexes in solution and analyse the relative stability of the "in-cage" and "out-of-cage" structures by using different spectroscopic techniques and DFT calculations.

Results and discussion

Synthesis of the ligands

The synthesis of H**no2th1tha** has been published previously.[24] The synthesis of H_2**no1th2tha** (**7**) started from orthoamide **3**,[25] which was converted to the **no1th** ligand (**5**) by alkylation with 2-(bromomethyl)thiazole followed by acid hydrolysis (Scheme 2). Compound **5** was then reacted with two equivalents of 2-chloromethylthiazolyl-4-carboxylic acid methyl ester, giving after purification and further acidic hydrolysis the expected ligand in 63% yield. H_3**no3tha** was synthesised by reacting 2-chloromethylthiazolyl-4-carboxylic acid methylester (3.3 equivalents) with tacn in acetonitrile, affording compound **1** in 87% yield after purification by chromatography. Acid hydrolysis of the ester functions with 6 M HCl gave H_3**no3tha** in its hydrochloride form in quantitative yield.

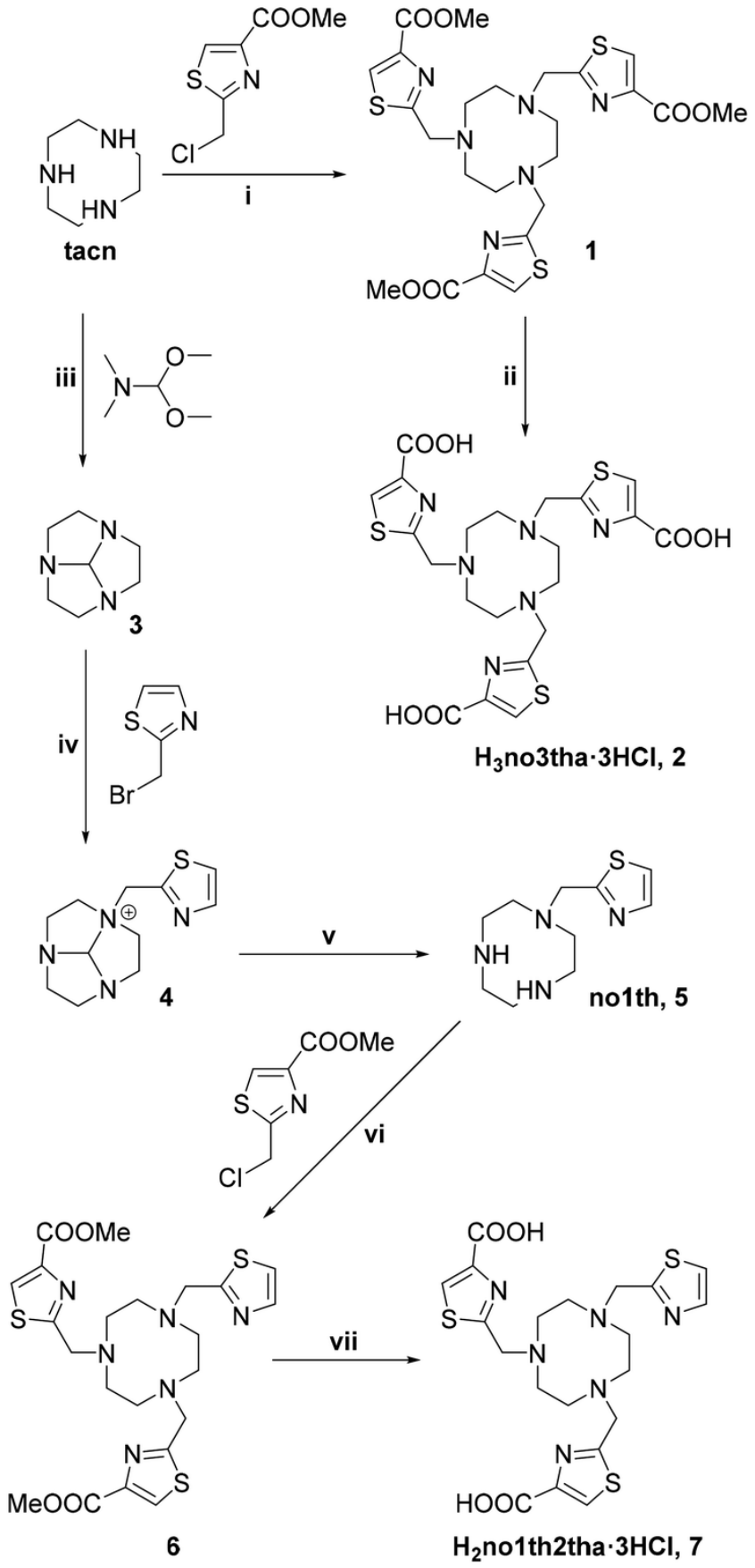

Scheme 2. Schematic synthesis of all compounds studied in this work. (i) K_2CO_3, CH_3CN, rt, 48 h; (ii) 6 M HCl, reflux, 24 h; (iii) $CHCl_3$/toluene (2/8), rt, 12 h; (iv) THF, rt, 20 h; (v) (1) 12 M HCl/MeOH (1/1), reflux, 24 h; (2) NaOH; (vi) K_2CO_3, CH_3CN, rt, 72 h; (vii) 6 M HCl, reflux, 24 h.

Acid–base behaviour of the ligands and their copper(ii) and zinc(ii) complexation properties

The acid–base behaviour of compounds H_2**no1th2tha** and H_3**no3tha** was studied by potentiometric titrations in aqueous solution at I = 0.10 ± 0.01 M of KNO_3 and 25.0 ± 0.1 °C. The results were compared to those previously reported for the H**no2th1tha** compound.[24] The stepwise constants K^H_i of the compounds in log units are presented in Table 1, while the overall protonation constants β^H_i (Table S1) and the corresponding species distribution diagrams (Fig. S18–S20) are reported in the ESI.

Table 1. Stepwise ($\log K^H_i$) protonation constants[a] of the studied ligands in aqueous solution at 25.0 ± 0.1 °C and I = 0.10 ± 0.01 M in KNO_3.

Equilibrium reaction[b]	H**no2th1tha**[c]	H_2**no1th2tha**	H_3**no3tha**	**no2th**[d]	H**tha**
$L + H^+ \rightleftarrows HL$	9.47	9.63(1)	9.58(1)	11.03	3.36
$HL + H^+ \rightleftarrows H_2L$	3.18	3.75(2)	3.90(1)	2.45	1.46
$H_2L + H^+ \rightleftarrows H_3L$	1.82	2.80(2)	3.26(1)	—	—
$H_3L + H^+ \rightleftarrows H_4L$	—	1.96(3)	2.22(1)	—	—
$H_4L + H^+ \rightleftarrows H_5L$	—	—	1.92(3)	—	—

[a] Values in parenthesis are the standard deviations in the last significant figures. [b] L denotes each ligand in general; the charges of ligand containing species are omitted for clarity. [c] From ref. 24. [d] From ref. 23.

The number of determined protonation constants increases with the number of carboxylic acid functions added to the methylthiazolyl arms. Indeed, H_2**no1th2tha** and H_3**no3tha** display four and five protonation constants, respectively, *versus* three for H**no2th1tha**. The first protonation constant is quite similar for the three ligands, at a $\log K$ of about 9.5, while the presence of a growing number of acid functions moderately increases the overall basicity of the ligands.

The first protonation constant corresponds to the protonation of one amine of the triazamacrocycle, and the second one to the protonation of a second amine of the ring.[26] The big decrease observed from the first to the second stepwise constant is due to the strong electrostatic repulsions of positive charges at short distances within the small triazamacrocycle, and surely the positive charges and consequently the protonation will be distributed among the three amines of the cycle.[27] An additional contributing factor is the electron withdrawing effect associated with the thiazolyl functions as seen before,[23,24] while no evidence of intramolecular hydrogen bonding was obtained. The following protonation constants can be attributed to the successive protonation of all carboxylate groups in the molecules.[24]

The complexation behaviour of H_2**no1th2tha** and H_3**no3tha** towards copper(ii) and zinc(ii) was also studied by potentiometric titrations under the experimental conditions used for the protonation studies, and compared to that of H**no2th1tha**. Potentiometric titrations were performed with each metal cation added at *ca.* 0.9 and 1.5 equiv. of the ligand amount, due to the potential formation of polynuclear complex species. The complexation of copper(ii) is very extensive with both ligands at low pH values, thus competition titrations with K_2H_2edta were additionally performed to determine the values of the stability constants for the ML species of both copper(ii) complexes. The complexation of zinc(ii) is also rather extensive with H_2**no1th2tha** but not with H_3**no3tha**, thus a competition titration with K_2H_2edta was only used in the former case. The values of the stability constants for the ML species obtained from the competition titrations were then kept fixed to calculate the remaining stability constants for each metal–ligand system, while using the combined titrations performed at different metal ratios. In this process it was found that all three ligands are

able to form copper(ii) complex species of 1 : 1 and 3 : 2 Cu^{2+}/L ratios, while for zinc(ii) complexes only species with a 1 : 1 Zn^{2+}/L ratio were found to form with each ligand. The stepwise constants ($\log K_{MmHhLl}$) obtained for all complexes are presented in Table 2, while the overall stability constants ($\log \beta_{MmHhLl}$) are compiled in Table S2 and species distribution diagrams calculated from these data are reported in Fig. 1 and Fig. S21–S23 (ESI). For copper(ii) the stability constants of the ML species decrease with an increasing number of methylthiazolylcarboxylate pendant arms on the ligand, while at the same time the stepwise constants of the M_3L_2 species conversely increase. For zinc(ii), the trend of decreasing constants for the ML species is even more striking.

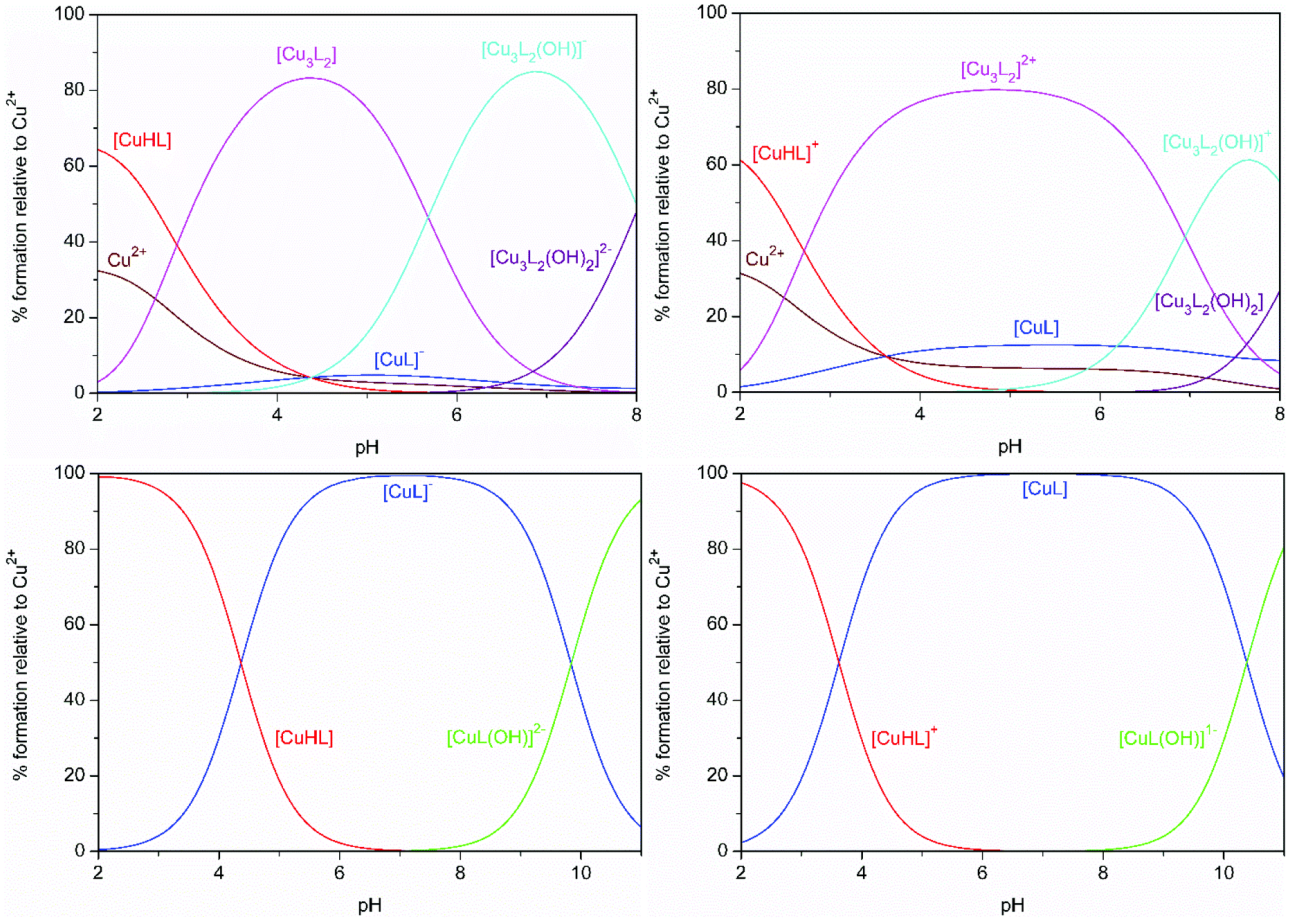

Fig. 1. Species distribution diagrams for the copper(ii) complexes of H_2**no1th2tha** (left) and H_3**no3tha** (right) at 1 : 1 (bottom) and 3 : 2 (top) Cu^{2+}/L ratios.

To better compare the complexation properties of the ligands pM values ($-\log [M^{2+}]_{free}$) were also calculated,[28] as they take into account the differing basicity of the ligands and the full set of stability constants for each system, see Table 2. The pM values show that the H**no2th1tha** ligand forms the most stable complexes with both copper(ii) and zinc(ii) and that the stability decreases in both cases with an increasing number of acid functions on the pendant arms. On the other hand, the selectivity for copper(ii) *versus* zinc(ii) (pCu – pZn) increases with the number of carboxylate functions. Comparing **no2th** directly with H**no2th1tha**, two ligands which only differ in the presence of the methylthiazolylcarboxylate pendant arm, one can observe that H**no2th1tha** provides a slightly better thermodynamic stability with copper(ii) than **no2th** but at the cost of a lower selectivity over zinc(ii).

Table 2. Stepwise ($\log K_{MmHhLl}$) stability constants,[a] and pM values[b] for the metal complexes of the studied ligands in aqueous solution at 25.0 ± 0.1 °C and I = 0.10 ± 0.01 M in KNO_3.

Equilibrium reaction[c]	H**no2th1tha**[d]	H_2**no1th2tha**	H_3**no3tha**	**no2th**[e]	**Htha**
$Cu^{2+} + 2\ L \rightleftarrows CuL_2$	—	—	—	—	9.09(2)
$CuL_2(OH) + H^+ \rightleftarrows CuL_2$	—	—	—	—	8.51(3)
$Cu^{2+} + L \rightleftarrows CuL$	19.8	18.0(1)[f]	16.6(1)[f]	20.77	—
$CuL + H^+ \rightleftarrows CuHL$	2.96	3.65(3)	4.38(3)	2.83	—
$CuL(OH) + H^+ \rightleftarrows CuL$	10.95	10.35(4)	9.81(2)	9.18	—
$2\ CuL + Cu^{2+} \rightleftarrows Cu_3L_2$	6.93	8.17(9)	9.28(7)	—	—
$Cu_3L_2(OH) + H^+ \rightleftarrows Cu_3L_2$	—	7.0(2)	5.7(1)	—	—
$Cu_3L_2(OH)_2 + H^+ \rightleftarrows Cu_3L_2(OH)$	—	8.3(2)	8.0(1)	—	—
$Zn^{2+} + L \rightleftarrows ZnL$	16.0	12.0(1)[f]	9.85(6)	16.28	—
$ZnL + H^+ \rightleftarrows ZnHL$	2.56	3.27(3)	7.38(2)	2.02	—
$ZnHL + H^+ \rightleftarrows ZnH_2L$	—	—	2.11(2)	—	—
$ZnL(OH) + H^+ \rightleftarrows ZnL$	11.15	11.04(5)	11.04(6)	10.53	—
pCu	17.74	15.80	14.44	17.15	5.33
pZn	13.89	9.77	7.96	12.65	—

[a] Values in parenthesis are the standard deviations in the last significant figures. [b] Calculated at $C_M = 1.0 \times 10^{-5}$ and 100% excess of ligand. [c] L denotes each ligand in general; the charges of ligand containing species are omitted for clarity. [d] From ref. 24. [e] From ref. 23. [f] Values determined from competition titrations with K_2H_2edta.

Looking at the potentiometric results with the ligand series, it is clear that the inclusion of methylthiazolylcarboxylate functions replacing methylthiazolyl ones favours the formation of polynuclear and likely "out-of-cage" complexes. Knowing the great impact of the macrocyclic effect in coordination chemistry, this means that the methylthiazolylcarboxylate arms have strong chelation properties that enter in competition with those of the tacn macrocycle. We thus investigated also the coordination properties of the free 4-thiazolecarboxylic acid ligand (H**tha**) towards copper(ii).

The acid–base and copper(ii) complexation properties of H**tha** were studied under the experimental conditions mentioned above, see Table 2. The H**tha** compound displays only highly acidic protonation centres as could be expected, the least acidic one likely corresponds to the carboxylic acid moiety of the compound. Concerning the copper(ii) complexation, it was found that H**tha** only forms 1 : 2 Cu^{2+}/L complex species, with CuL_2 exhibiting a stability constant in agreement with the stepwise stability constants of the Cu_3L_2 species obtained with the series of three tacn ligands.

Synthesis of the complexes and structural studies

Considering the potentiometric results, the synthesis of the copper(ii) and zinc(ii) complexes of the macrocyclic ligands was pursued with the aim of isolating the ML species and also the M_3L_2 species by using 1.5 equiv. of the metal salts. The synthesis of complexes was performed in water, using an appropriate amount of metal perchlorate at pH 6–7, and they were isolated in a solid form after careful evaporation of solvent and methanol rinses.

Single crystals suitable for X-ray studies were obtained for some complexes. Depending on the ligand, X-ray structures containing mono- or tri-nuclear complexes were isolated. The H**no2th1tha** ligand allowed us to isolate the M_3L_2 species by slow evaporation of a saturated aqueous solution containing the M_3L_2 complex, while for H_3**no3tha**, both species were obtained by slow evaporation of saturated aqueous solutions containing either the ML or M_3L_2 species. The details of the different structures are described below.

Crystals of $[Cu_3(\mathbf{no2th1tha})_2(ClO_4)_2](ClO_4)_2$ contain the centrosymmetric trinuclear $[Cu_3(\mathbf{no2th1tha})_2(ClO_4)_2]^{2+}$ entity and two perchlorate counter ions. A view of the structure of the complex is shown in Fig. 2, while the bond distances of the coordination environments are gathered in Table 3. Two of the Cu centres, labelled as Cu1, are each coordinated by three nitrogen atoms of a tacn unit, and the five-coordination is completed by two nitrogen atoms from two methylthiazolyl pendant arms. The metal coordination environments around the Cu1 centres can be described as square pyramidal, where N2, N3, N5 and N6 define the basal plane (mean deviation from planarity of 0.101 Å) and N1 occupies the apical position. The metal ions are placed 0.286 Å above the basal plane, while the bond distance involving the apical donor atom is longer than those involving the donor atoms of the basal plane, as usually observed for square pyramidal copper(ii) complexes.[29] The overall coordination environments of the metal centres labelled as Cu1 are very similar to that reported previously for $[Cu(\mathbf{no2th})]^{2+}$.[23]

Table 3. Bond distances (Å) of the metal coordination environments of the indicated complexes obtained from X-ray diffraction measurements.

	$[Cu_3(\mathbf{no2th1tha})_2(ClO_4)_2]^{2+}$	$[Cu_3(H\mathbf{no3tha})_2(ClO_4)_2]$	$[Cu(H\mathbf{no3tha})]$	$[Zn(H\mathbf{no3tha})]$	$[Cu(\mathbf{tha})_2]$	$[Cu(\mathbf{tha})_2]\cdot 4H_2O$
M1–N1	2.218(6)	2.026(4)			1.960(4)	1.974(2)
M1–N2	2.031(6)	2.060(4)				
M1–N3	2.069(7)	2.330(4)				
M1–N4		2.042(4)	2.087(2)	2.284(7)		
M1–N5	1.977(7)	2.692(5)	2.066(2)	2.233(7)		
M1–N6	1.963(6)		2.430(2)	2.190(7)		
M1–O1			2.309(2)	2.062(6)	1.949(3)	1.9620(18)
M1–O2					2.882(3)	2.567(2)
M1–O3			1.984(2)	2.057(7)		
M1–O5			1.981(2)	2.069(6)		
M1–O7		1.952(3)				
M2–N4	2.015(6)					
M2–N6		2.015(4)				
M2–O1	1.923(5)					
M2–O5		1.915(4)				
M2–O7	2.701(4)					
M2–O10		2.745(10)				

The third Cu centre in $[Cu_3(\mathbf{no2th1tha})_2(ClO_4)_2]^{2+}$ is coordinated to two thiazolylcarboxylate groups from two different ligands. The coordination environment around Cu2 can be described as octahedral with a severe axial elongation associated with the Jahn–Teller effect. The strictly planar equatorial plane is defined by the N and O donor atoms of the thiazolylcarboxylate groups, and contains the metal ion. The axial positions are occupied by the oxygen atoms of two perchlorate anions providing a weak interaction with the metal ion. Similar weak axial coordination of perchlorate groups was observed previously for different copper(II) complexes.[30] The *cis* angles of the equatorial plane of 96.3(2)° and 83.7° differ considerably from the ideal value of 90° as a result of the small bite angle of the thiazolylcarboxylate unit.

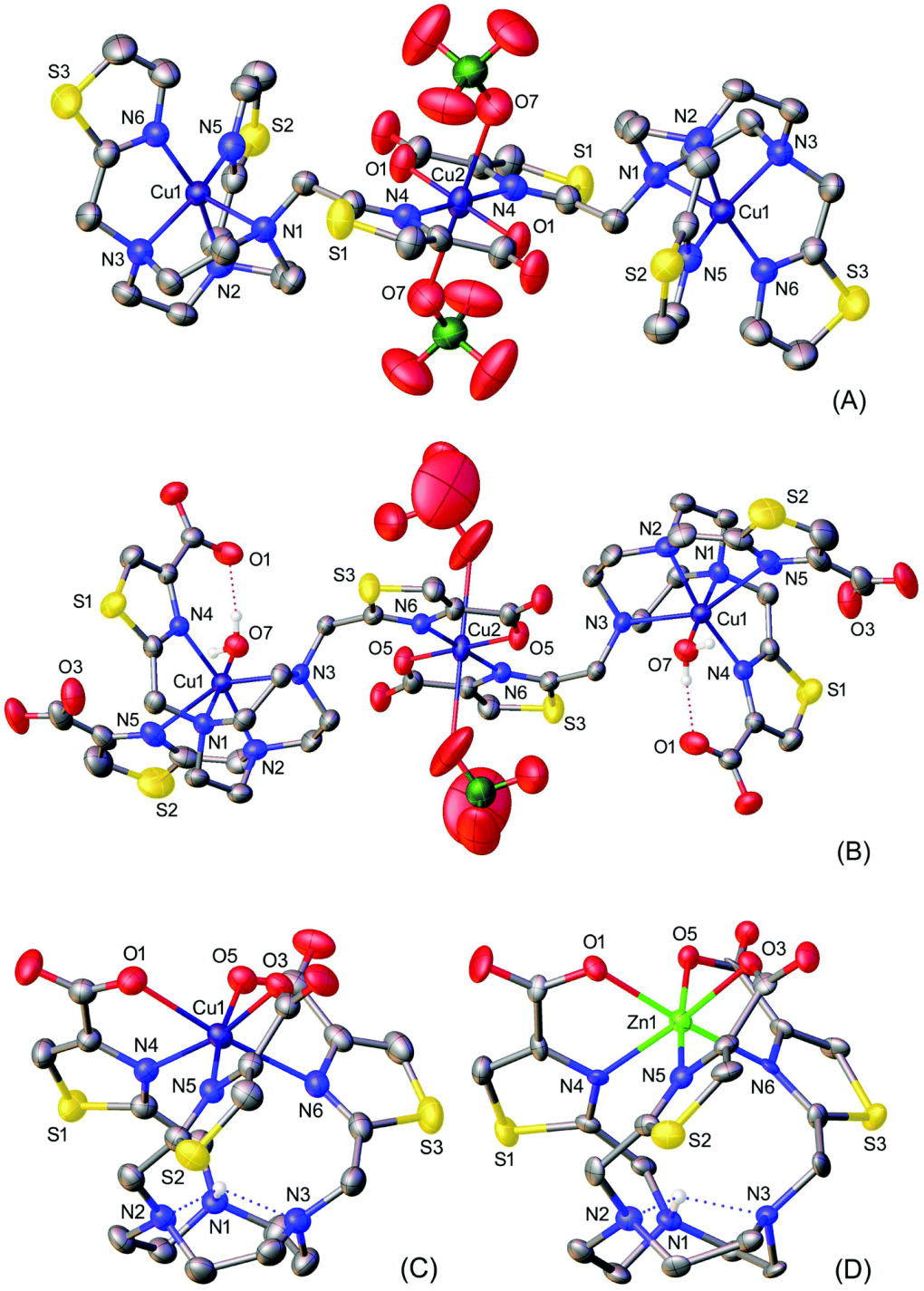

Fig. 2. Views of the X-ray structures of the complexes $[Cu_3(\mathbf{no2th1tha})_2(ClO_4)_2]^{2+}$ (A), $[Cu_3(\mathbf{no3tha})_2(ClO_4)_2]^{2-}$ (B), [Cu(H**no3tha**)] (C) and [Zn(H**no3tha**)] (D). Hydrogen atoms and counterions are omitted for clarity. The ORTEP plots are at the 50% probability level.

The trinuclear $[Cu_3(H\mathbf{no3tha})_2(ClO_4)_2]$ complex presents a structure similar to that of the H**no2th1tha** analogue. The coordination environment around Cu2 mimics that found in the H**no2th1tha** analogue, the main difference being the longer axial Cu–O distances involving the perchlorate groups in the complex with H_3**no3tha** (Table 3). The Cu1 ions are coordinated to the three nitrogen atoms of the tacn unit (N1, N2 and N3) and two nitrogen atoms of the thiazolylcarboxylate pendants (N4 and N5). The hexacoordination is completed by the presence of an inner-sphere water molecule. The coordination polyhedron can be described

as an axially distorted octahedron. The equatorial plane is defined by N1, N2, N4 and O7, while the axial positions are occupied by N3 and N5, which are characterised by longer Cu–N bonds (Table 3). One of the thiazolylcarboxylate units of each ligand is protonated, which is reflected in rather different C16–O3 and C16–O4 distances (1.301(8) and 1.220(7) Å, respectively).

The structures of [Cu(H**no3tha**)] and [Zn(H**no3tha**)] are very similar. The metal ions are coordinated to the three pendant arms of the ligand, yielding a N_3O_3 exocyclic coordination. One of the nitrogen atoms of the tacn unit is protonated, which likely favours the exocyclic coordination.

The octahedral coordination polyhedron in [Cu(H**no3tha**)] is again distorted as a result of the Jahn–Teller effect, with two long axial distances (Cu–N6 and Cu–O1, Table 3) and four shorter distances involving the donor atoms of the equatorial plane (mean deviation from planarity of 0.01°). The *trans* angles (O5–Cu–N5, 170.40(9)°; O3–Cu–N4, 167.83(9)°; O1–Cu–N6, 174.39(8)°) show moderate deviations from the ideal value of 180°, while the *cis* angles fall within the range 76.3 to 106.0°. In the Zn structure the bond distances of the metal coordination environment fall within a narrower range (2.06–2.28 Å compared to 1.98–2.43 Å) than that observed for the Cu analogue.

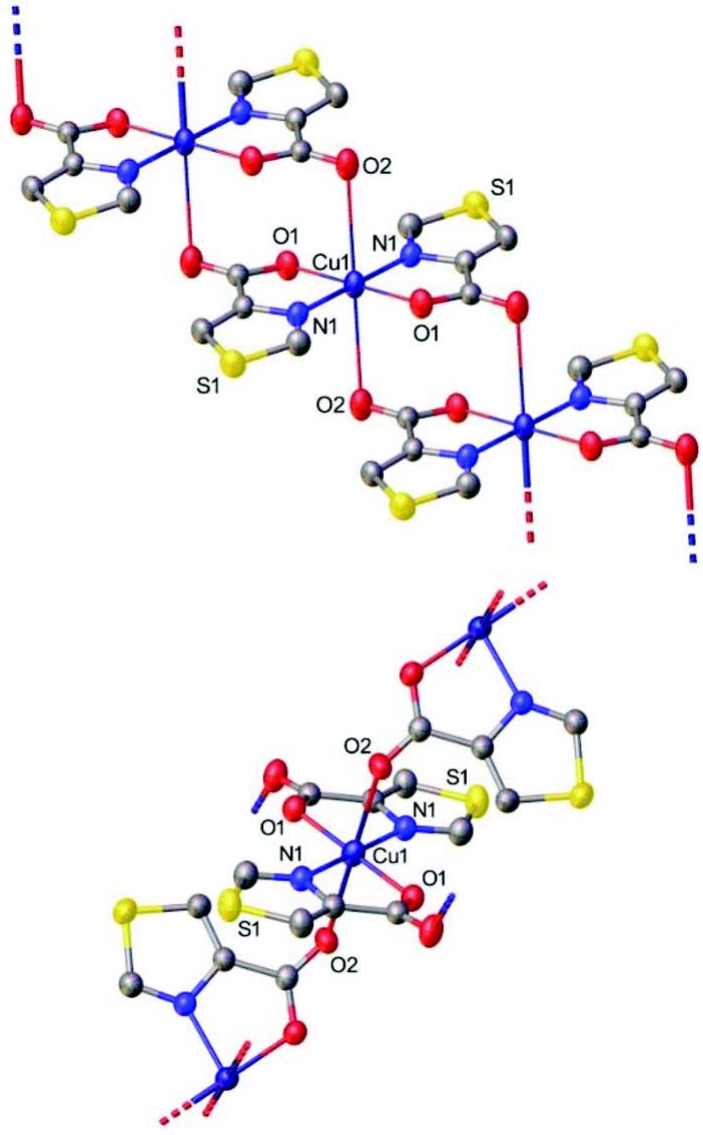

Fig. 3. Views of the X-ray structures of [Cu(**tha**)$_2$] (top) and [Cu(**tha**)$_2$]·4H_2O (bottom). Hydrogen atoms and counterions are omitted for clarity. The ORTEP plots are at the 50% probability level.

The copper(II) complex of methylthiazolylcarboxylate (H**tha**) was also synthesised as a model system for the exocyclic coordination described above, and single crystals suitable for X-ray diffraction were also obtained by slow evaporation of the complexes in water. The [Cu(**tha**)$_2$] complex was crystallised in two different forms, both in the monoclinic $P2_1/c$ space group, with one of them containing water molecules in the crystal lattice (Fig. 3). The structures obtained under our conditions are very similar to those already described,[31] showing the efficiency of such chelating units to form polynuclear networks. The two structures contain square-planar [Cu(**tha**)$_2$] units with the copper centre lying on a crystallographic inversion centre, being coordinated by two nitrogen atoms and two oxygen atoms from two inversion-related **tha**$^-$ ligands. The [Cu(**tha**)$_2$] units are joined by weak Cu···O interactions [Cu···O2 = 2.567(2) and 2.882(3) Å for [Cu(**tha**)$_2$]·4H$_2$O and [Cu(**tha**)$_2$], respectively], which expand the coordination of the metal ion into a 4 + 2 mode, as observed previously for copper(II) complexes of pyrazinecarboxylate,[32] 4,4′-bipyridine-2-carboxylate[33] and pyridine-2,6-dicarboxylate.[34] The metal coordination environments in these two forms of the [Cu(**tha**)$_2$] complex are very similar to those found around the Cu2 metal centres in the trinuclear species [Cu$_3$(**no2th1tha**)$_2$(ClO$_4$)$_2$]$^{2+}$ and [Cu$_3$(**no3tha**)$_2$(ClO$_4$)$_2$]$^{2-}$, which together with the similarity of the stability constants in solution explains why such trinuclear species are so easily formed in the presence of an excess of Cu^{2+} for ligands containing at least one thiazolylcarboxylate pendant arm.

Spectroscopic and computational studies

Absorption spectra in the visible region at 25 °C were obtained from aqueous sample solutions of the copper(II) complexes of the three macrocyclic ligands containing a 1 : 1 or 1.5 : 1 Cu^{2+}/L ratio. All copper(II) complexes exhibit a single wide absorption band with maxima varying from 650 to 670 nm and a low intensity, which is characteristic of d–d transitions of Cu^{2+} in square pyramidal or distorted octahedral environments.[35] The samples containing more than 1 equiv. of Cu^{2+} did not display any significant change relative to the ones at a 1 : 1 ratio. Thus, the trinuclear species mentioned before could not be identified by visible absorption. The wavelengths and intensity for the absorption maxima reported in Table 4 are those observed for the samples containing the 1 : 1 Cu^{2+}/L ratio.

Table 4. Visible absorption bands,[a] EPR parameters[b] obtained from the simulation of the experimental spectra and EPR parameters obtained with DFT calculations for the copper(II) complexes studied in this work.

		λ_{max}/nm (ε /M^{-1} cm^{-1})	g_x	g_y	g_z	A_x	A_y	A_z
Hno2th1tha	Exp.	650 (116)	2.040	2.071	2.208	1	27	183
	Calcd		2.062	2.064	2.187	16.3	21	174[b]
H2no1th2tha	Exp.	655 (158)	2.036	2.084	2.228	24	35	164
H3no3tha	Exp.	670 (73)	2.043	2.078	2.244	8	23	175
	Calcd[c]		2.063	2.085	2.218	13	42	181
	Calcd[d]		2.045	2.071	2.177	4.0[f]	29	186[b]
	Calcd[e]		2.047	2.074	2.185	5.0[f]	32	178[b]
Htha			2.056	2.072	2.276	1	11	174

[a] λ_{max} in nm and ε in M^{-1} cm^{-1}. [b] A_i given in 10^{-4} cm^{-1}. [c] Calculated for the *exo*-cyclic [Cu(**no3tha**)]$^-$ complex. [d] Calculated for the *endo*-cyclic [Cu(**no3tha**)(H$_2$O)]$^-$ complex. [e] Calculated for the *endo*-cyclic [Cu(**no3tha**)]$^-$ complex. [f] Calculated as negative values.

The EPR spectra of the above complexes were obtained at 130 K from frozen aqueous solutions at 1 M NaClO$_4$. The spectra (Fig. 4) could all be simulated using a single paramagnetic species, as no evidence of

additional species with different structures was distinguishable in the spectra. The spectra show at least three of the four lines expected for g_z, with the superhyperfine interactions due to the presence of the nitrogen atoms not being observed. The values of the g factors and the A hyperfine coupling constants obtained by simulation of the experimental spectra (Table 4) indicate three different principal values of g, with $g_z > (g_x + g_y)/2$ and the lowest $g \geq 2.04$, characteristic of mononuclear copper(II) complexes in a rhombic symmetry with elongation of the axial bonds and a $d_{x^2-y^2}$ ground state. Combined with the maxima and intensity of the visible absorption bands, these data are consistent with distorted square pyramidal or octahedral geometries.[36]

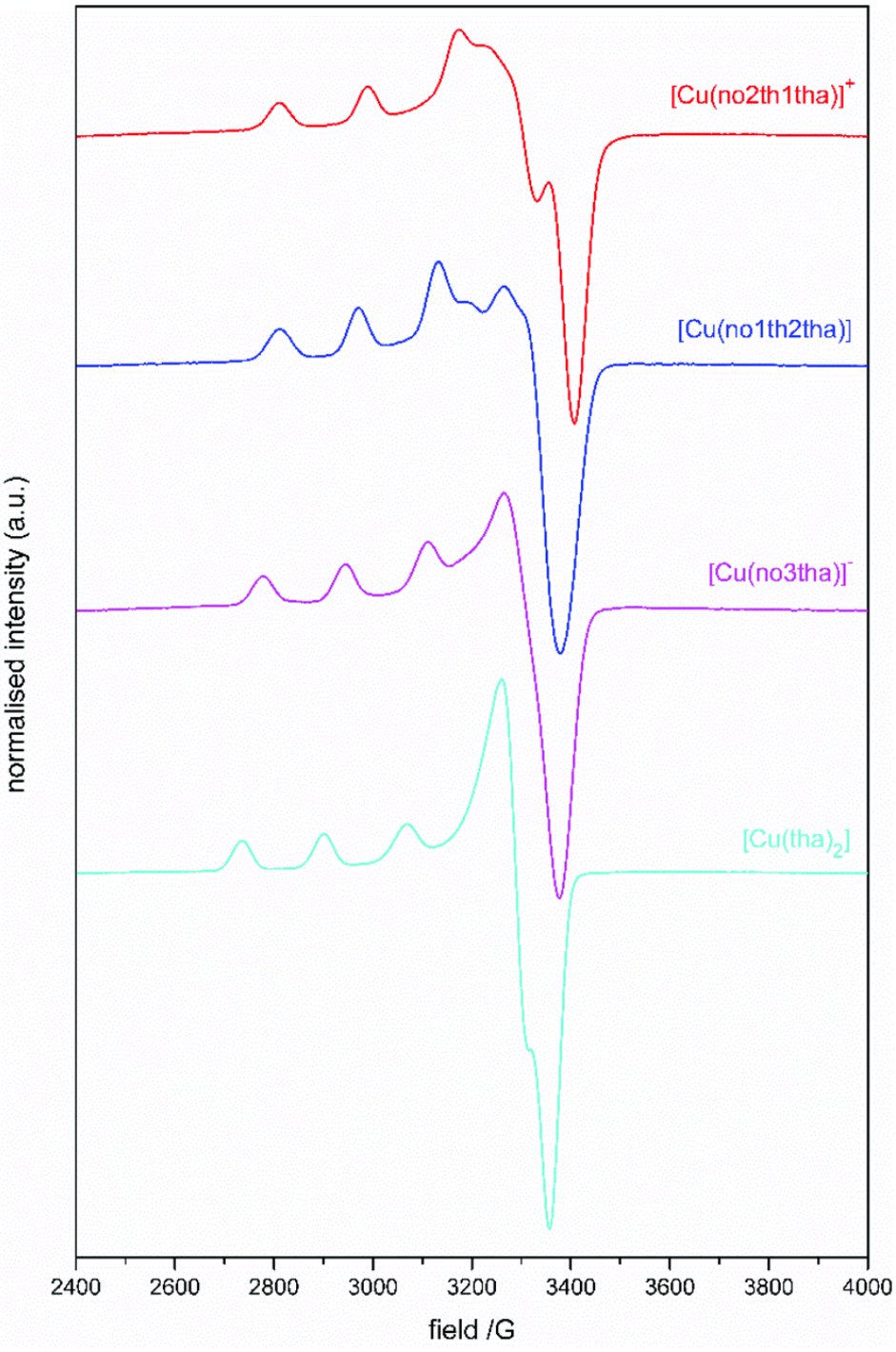

Fig. 4. EPR spectra for the 1 : 1 ratio copper(II) complexes of the studied ligands in aqueous solutions at 1 M in $NaClO_4$ and pH = 7.0.

Solutions of the copper(II) complexes of H**tha** containing either a 1 : 3 or 1 : 2 Cu^{2+}/L ratio were also prepared in 1 M $NaClO_4$ medium and the EPR spectra of the corresponding frozen samples were acquired at 130 K. Both spectra are analogous and could also be simulated using a single paramagnetic species, thus the one for the 1 : 2 Cu^{2+}/L ratio was taken as the representative (Fig. 4). This spectrum is relatively similar to those of the complexes of the triaza ligands (Table 4), being also characteristic of mononuclear copper(II) complexes in a rhombic symmetry with elongation of the axial bonds and a $d_{x^2-y^2}$ ground state. The only difference between these spectra and the previous ones is the noticeably higher value obtained for the g_z parameter, at around 2.28–2.29 instead of 2.21–2.25, which points to the participation of several oxygen atoms at equatorial coordination positions.[37] A significant increase of g_z is also observed when comparing the data obtained for [Cu(**no2th1tha**)]$^+$ and [Cu(**no3tha**)]$^-$, again suggesting an increasing number of oxygen donor atoms involved in coordination to the metal ion. The EPR spectra of the macrocyclic complexes remain nearly unaffected by the addition of Cu^{2+} to reach a 3 : 2 (M : L) ratio, likely as a result of the very similar spectra of the *endo*- and *exo*-cyclic metal centres.

In order to characterise the complexes in solution by ^{1}H NMR, we used the corresponding diamagnetic Zn(II) analogues in place of the paramagnetic Cu(II) complexes of H_3**no3tha** and H_2**no1th2tha**. The spectra were recorded in D_2O at 25 °C and compared to those of the free ligands (Fig. S9 and S12, ESI). The spectrum of the [Zn(H**no3tha**)] complex evidences a slight shielding of the peaks corresponding to the methylene protons of the triazamacrocycle, which are observed as two signals because of the different environments of the proton nuclei originated by the complexation with Zn(II). A slight upfield shift ($\Delta\delta$ = 0.22 ppm) of the signal due to the thiazolyl group is also observed. It is noteworthy that the signal of the CH_2 protons of the pendant arms is observed as a singlet. In contrast, the ^{1}H NMR spectrum of [Zn(**no1th2tha**)] is characteristic of a more rigid structure. In particular, two of the CH_2 groups of the pendant arms give an AB spin system with doublets at 4.42 and 4.56 ppm, while the CH_2 group of the third arm gives a singlet at 4.52 ppm. This suggests that one of the pendant arms is not involved in coordination to the metal ion. The more rigid structure evidenced by the ^{1}H NMR spectrum of [Zn(**no1th2tha**)] suggests an endocyclic coordination of the metal ion, while for [Zn(H**no3tha**)] the spectrum is compatible with the exocyclic coordination observed in the solid state. This *exo*-cyclic coordination is compatible with the rather high protonation constant determined by potentiometric titrations (log K_{ZnHL} = 7.38), which can only be explained by the protonation of the tacn unit.

In order to gain further insight into the structure of the complexes in solution, we performed DFT calculations at the TPSSh/Def2-TZVPP level (see computational details below). We initially performed geometry optimizations on the [Cu(**no3tha**)]$^-$·H_2O system, which provided two local energy minima with the Cu^{2+} ion showing either *endo*- or *exo*-cyclic coordination, with the metal coordination environments being very similar to those observed in the solid state for the [Cu_3(H**no3tha**)$_2$(ClO_4)$_2$] and [Cu(H**no3tha**)] complexes (Fig. S28, ESI). The corresponding relative Gibbs free energy favoured the exocyclic coordination by 6.2 kcal mol^{-1}. The exocyclic form becomes even more stable with respect to the endocyclic one in the absence of the additional water ligand (11.2 kcal mol^{-1}). These results strongly support that the [Cu(**no3tha**)]$^-$ complex presents an exocyclic coordination similar to that observed for the protonated complex in the solid state.

Theoretical calculations of the EPR parameters using DFT methods gave additional support to the proposed exocyclic coordination in [Cu(**no3tha**)]$^-$. In particular, our calculations give EPR parameters for the *endo*-cyclic [Cu(**no3tha**)(H_2O)]$^-$ and [Cu(**no3tha**)]$^-$ model systems that are virtually identical to those calculated for [Cu(**no2th1tha**)]$^+$, which was previously demonstrated to present an endocyclic structure (Table 4).[24] Conversely, the exocyclic form of the [Cu(**no3tha**)]$^-$ complex presents a significantly higher value of g_z, in line with the experimental values. The calculated *g*-tensor contains contributions from the relativistic mass correction, the diamagnetic spin–orbit term, and the paramagnetic spin−orbit term, with the latter representing the main contribution (Table S2, ESI). The higher g_z value calculated for the *exo*-cyclic

[Cu(**no3tha**)]$^-$ system compared to [Cu(**no2th1tha**)]$^+$ is the result of a larger paramagnetic spin−orbit contribution, which correlates well with the simultaneous red shift of the d−d absorption bands in the electronic spectra (Table 4).

Electrochemical properties

The redox properties of the [Cu(**no1th2tha**)] and [Cu(**no3tha**)]$^-$ complexes were studied by cyclic voltammetry (CV) in aqueous solutions of 0.1 M $LiClO_4$ at pH ∼7 at a glassy carbon electrode under argon (Fig. 5, A1–2 and B1–2). The electrochemical parameters are gathered in Table 5, together with those of [Cu(**no2th1tha**)](ClO_4) and [Cu(**no2th**)](ClO_4)$_2$ for the sake of comparison. The cyclic voltammogram of [Cu(**no3tha**)]$^-$ displays an irreversible system behaviour with E_{pc} = −0.48 V and E_{pa} = −0.26V with a high ΔE value of 0.22 V, suggesting that coordination modifications occurred in the system after reduction (Fig. 5, B1). By contrast, the CV of the [Cu(**no1th2tha**)] complex, carried out under the same conditions, exhibits a quasi-reversible system behaviour with E_{pc} = −0.31 V and E_{pa} = −0.19 V (ΔE_p = 0.12 V) (Fig. 5, A1). In the last case, a second weak oxidation peak can be noted (E_{pa2} = 0.14 V) on the back scan, revealing that a very minor part of the formed Cu(I) complex might undergo a system reorganisation.

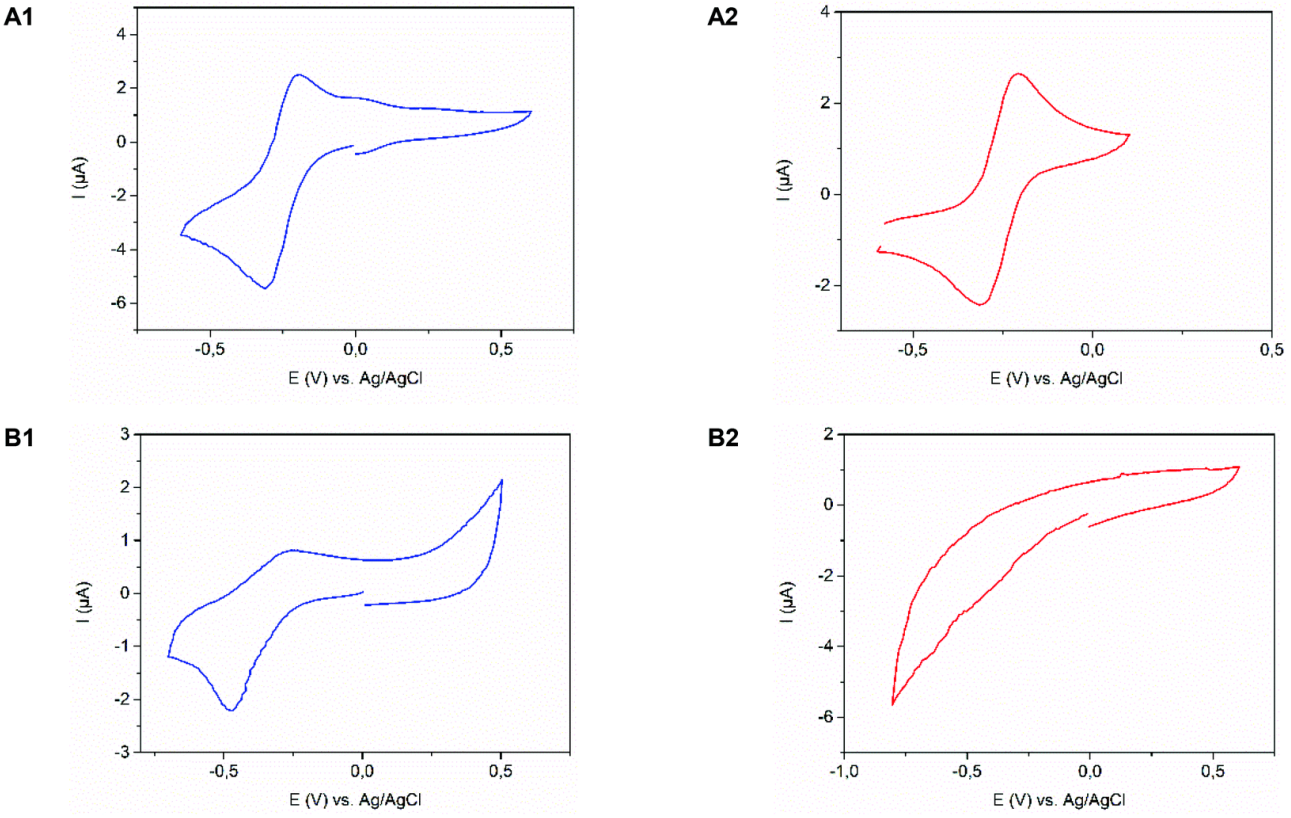

Fig. 5. Cyclic voltammograms (0.1 V s^{-1} scan rate) before (A1, B1) and after (A2, B2) electrolysis of complexes at a glassy carbon electrode in 0.1 M H_2O/$LiClO_4$ under an argon atmosphere; A: 1 mM [Cu(**no1th2tha**)], pH 7.1; B: 1 mM [Cu(**no3tha**)]$^-$, pH 6.8.

Electrolyses of the two complexes were performed to further evaluate the stability of the Cu(I) species. For [Cu(**no3tha**)]$^-$, the CV of the resulting Cu(I) complex after electrolysis at $E°$ = −0.55 V shows no oxidation or reduction waves, indicating that demetallation occurred, in agreement with the previously observed irreversible behaviour (Fig. 5, B2). This might be related to the *exo*-cyclic coordination of the metal ion

suggested by X-ray and computational studies. For the second complex [Cu(**no1th2tha**)], the CV of the Cu(I) species obtained after electrolysis at $E°$ = −0.40 V (*vs.* Ag/AgCl) confirmed the quasi-reversible character of this new system (Fig. 5, A2).

The [Cu(**no2th1tha**)]$^{+}$ and [Cu(**no1th2tha**)] complexes exhibit close redox properties (Table 5) with similar voltammetric profiles. Nevertheless, [Cu(**no2th**)]$^{2+}$ presents the most negative $E_{1/2}$ value (−0.47 V *vs.* Ag/AgCl) within this series of complexes, and appears to be the most stable one in the presence of potential reducing agents.

Table 5. Electrochemical data (in *V vs.* Ag/AgCl) measured for the studied copper(II) complexes.

Ligand	E_{pc}	E_{pa}	$E_{1/2}$	ΔE
no2th[a]	−0.51	−0.44	−0.47	0.07
Hno2th1tha[b]	−0.32	−0.23	−0.27	0.09
H_2no1th2tha	−0.31	−0.19	−0.26	0.12
H_3no3tha	−0.48	−0.26	-	0.22

[a] From ref. 23. [b] From ref. 24.

Conclusions

Following our earlier study on the Cu(II) complexation with the H**no2th1tha** azaligand, in which potentiometric titrations evidenced the formation of Cu_3L_2 species depending on the stoichiometric conditions,[24] we have investigated the complexation properties of close tacn-based ligands bearing an increased number of methylthiazolylcarboxylate arms. We reasoned that the presence of such coordinating arms should have an important impact on copper coordination, in particular promoting the formation of polynuclear and *exo*-cyclic structures.

The potentiometry study has revealed that the two newly synthesised chelators H_2**no1th2tha** and H_3**no3tha** also lead to trinuclear M_3L_2 complexes with copper(II) but mononuclear ML complexes with zinc(II). Complexes of this ligand series have been synthesised and some of them have been isolated and characterised by X-ray diffraction. This allowed us to elucidate the structures of the polynuclear complexes and to determine the tendency of such ligands to form preferentially exocyclic over endocyclic complexes by increasing the number of methylthiazolylcarboxylate arms and/or the stoichiometric amount of metal.

The trimetallic [Cu_3(**no2th1tha**)$_2$(ClO_4)$_2$](ClO_4)$_2$ and [Cu_3(H**no3tha**)$_2$(ClO_4)$_2$] structures are composed of two ligands exhibiting a cupric endocyclic cation in each macrocycle, while the third copper centre is coordinated jointly by a methylthiazolylcarboxylate unit of each macrocycle. This tendency could be explained by looking at the mononuclear [Cu(H**no3tha**)] and [Zn(H**no3tha**)] structures, which contain a metal centre coordinated in an exocyclic manner by the three methylthiazolylcarboxylate pendants. This chelator then promotes the formation of "out-of- cage" complexes, at least in the absence of an excess of metal.

The analysis of the structures of the complexes in solution using visible absorption and EPR spectroscopy also suggests the change from *endo*- to *exo*-cyclic coordination shown in the solid state. DFT calculations also support the exocyclic coordination mode with copper(II) of the H_3**no3tha** ligand. NMR experiments that are limited to the Zn(II) complexes are in accordance with an endocyclic complex with H_2**no1th2tha**, while

the NMR spectra of [Zn(H**no3tha**)] give evidence of an exocyclic coordination, confirming the previous behaviour. Nevertheless, as demonstrated by the electrochemical study of the copper complexes, the "out of cage" complexes are not stable regarding the Cu(II)–Cu(I) reduction when compared to their "in cage" analogue.

This study confirmed that H**no2th1tha** is a promising bifunctional chelator for conjugation, as we demonstrated on a previous report.[24] It has also shown that methylthiazolylcarboxylate pendant arms attached to a tacn scaffold can compete with the small triazamacrocycle unit for copper(II) coordination, as their number increases. This leads to exocyclic complexation when the number of thiazolylcarboxylate groups alone satisfies the coordination sphere of the cation, counterbalancing the macrocyclic effect. Finally, this study has evidenced that methylthiazolylcarboxylate coordinating groups are strong chelating units and thus should be of great interest for their incorporation into non-macrocyclic chelators.

Experimental section

Materials and methods

Reagents were purchased from ACROS Organics and from Aldrich Chemical Co. 1,4,7-Triazacyclononane (tacn) was purchased from CheMatech (Dijon, France). 2-Bromomethylthiazole[38] and 2-chloromethyl-1,3-thiazole-4-carboxylic acid methyl ester were obtained by following the published procedures.[39] Acetonitrile, THF and water solvents were distilled before use. HRMAS analyses were performed at ICOA, Orléans, France. NMR spectra were recorded at the "Services communs" of the University of Brest. ^{1}H and ^{13}C NMR spectra were recorded with Bruker Avance 500 (500 MHz), Bruker Avance 400 (400 MHz), or Bruker AMX-3300 (300 MHz) spectrometers. Chemical shifts in NMR are given in ppm (δ) and coupling constants (J) in Hz.

Ligand synthesis

1,4,7-tris(methylthiazol-2-ylmethyl-4-carboxylate)-1,4,7-triazacyclononane (no3tha). 2-Chloromethyl-1,3-thiazole-4-carboxylic acid methyl ester (1.71 g, 12.7 mmol, 3.3 eq.) was added to a solution of tacn (500 mg, 3.80 mmol) in 40 mL of CH_3CN with potassium carbonate (3.15 g, 22.8 mmol). The mixture was stirred at room temperature for 2 days. The mixture was filtered over a Celite pad and the filtrate was evaporated under dryness. The residue was purified by flash chromatography on silica gel ($CHCl_3$ 100% to $CHCl_3$/MeOH 90 : 10) yielding a yellow oil (2.0 g, 87%). **^{1}H NMR** (300 MHz, $CDCl_3$) δ 2.96 (s, 12H, CH_2 tacn), 3.91 (s, 9H, CH_3), 4.03 (s, 6H, CH_2αN), 8.13 (s, 3H, CH); **^{13}C NMR** (75.5 MHz, $CDCl_3$) δ 52.5 (CH_3), 56.3 (CH_2 tacn), 60.4 (CH_2); 128.4 (CHαS), 146.5 (C=N), 161.9 (CO), 173.7 (Cq); **ESI-HRMS***m*/*z* calcd for $[C_{24}H_{31}N_6O_6S_3]^+$ 595.14617, found 595.14557.

The previous yellow oil was dissolved in 6 M hydrochloric acid and stirred under reflux for 24 hours. Evaporation of the aqueous solvent gave 1,4,7-tris(methylthiazol-2-ylmethyl-4-carboxylate)-1,4,7-triazacyclononane H_3**no3tha**·3HCl in its hydrochloride salt as a white solid in quantitative yield (2.10 g). ^{1}H NMR (300 MHz, D_2O) δ 3.48 (s, 12H, CH_2 tacn), 4.61 (s, 6H, CH_2αN), 8.34 (s, 3H, CH); ^{13}C NMR (75.5 MHz, D_2O) δ 53.5 (CH_2 tacn), 58.5 (CH_2), 134.2 (CHαS), 148.7 (CαCO), 166.3 (CO), 168.0 (C=N). ESI-HRMS: *m*/*z* calcd for $[C_{21}H_{25}N_6O_6S_3 + H]^+$ 553.09925, found 553.09922 [M + H^+].

1-Methylthiazolyl-1,4,7-triazacyclononane (no1th). *N*-Dimethoxymethyl-*N*,*N*-dimethylamine (1.1 g, 9.28 mmol) was added to a solution of tacn (1.2 g, 9.28 mmol) in a mixture of $CHCl_3$/toluene 2/8 v/v (10 mL). The reaction mixture was stirred at room temperature for 12 h, and the solvent was then evaporated under reduced pressure yielding **3** as a clear oil in quantative yield (1.28 g, 99%). The protected tacn[25] (1.10 g, 7.90 mmol) was dissolved in the minimum amount of THF (10 mL) and then a solution of 2-

(bromomethyl)thiazole (1.90 g, 10.2 mmol) in THF (3 mL) was added. The reaction mixture was stirred at room temperature for 20 hours. The precipitate was filtered to yield **4** as a yellow powder (2.20 g, 89%). The corresponding ammonium salt (887 mg, 3.49 mmol) was dissolved in 12 M HCl/MeOH 1/1 v/v (20 mL) and stirred at reflux for 24 hours. After evaporation of the solvent, the crude product was dissolved in water and the pH of the aqueous solution was adjusted to pH >12 with NaOH pellets. The aqueous solution was extracted with CH_2Cl_2 (3 × 30 mL), the combined organic layers were dried over $MgSO_4$, and evaporated to yield **no1th** as a brown oil (791 mg, 99%). ^{1}H NMR (D_2O, 300 MHz, 298 K) δ 2.68 (m, 4H), 2.98 (m, 4 H), 3.24 (s, 4H, CH_2–N), 4.15 (s, 2H), 7.70 (d, 1H, *J* 3), 7.80 (d, 1H, *J* 3). ^{13}C NMR (D_2O, 75.5 MHz, 298 K) δ 44.7, 46.1, 49.7 (CH_2 tacn), 53.7 (CH_2-N) 127.9 (CH), 136.4 (CH), 171.4 (Cq). ESI-HRMS *m*/*z* calcd for $C_{10}H_{19}N_4S$, 227.13249; found, 227.13257.

1-(Thiazol-2-ylmethyl)-4,7-bis(methyl-thiazol-2-ylmethyl-4-carboxylic acid)-1,4,7-triazacyclononane, H_2no1th2tha (7). A solution of 2-chloromethyl-1,3-thiazole-4-carboxylic acid methyl ester (1.35 g, 7.32 mmol) in acetonitrile (60 mL) and potassium carbonate (4.05 g, 29.3 mmol) were added to **no1th** (791 mg, 3.49 mmol) dissolved in acetonitrile (20 mL). The mixture was stirred at room temperature for 3 days, filtered and the solvent was evaporated under reduced pressure to yield a brown oil. The residue was purified by flash chromatography on Al_2O_3 (hexane/$CHCl_3$ 70 : 30 to 30 : 70) yielding **6** as a yellow oil (1.35 g, 72%). ^{1}H NMR (300MHz, $CDCl_3$) δ 2.92–2.99 (m, 12H, CH_2 tacn), 3.91 (s, 6H, CH_3), 4.02 (s, 6H), 7.25 (d, 1H, *J* 3), 7.64 (d, 1H, *J* 3), 8.12 (s, 1H); ^{13}C NMR ($CDCl_3$, 75.5 MHz, 298 K) δ 52.5 (CH_3), 56.1, 56.2, 56.4 (CH_2 tacn), 60.2 (CH_2), 119.4 (CH αS), 128.4 (CH αS), 142.3 (CH αN), 146.4 (Cq), 162.0 (C=O), 171.5 (Cq), 174.0 (Cq); ESI-HRMS *m*/*z* calcd for $C_{22}H_{29}N_6O_4S_3$, 537.14069; found, 537.14088.

Compound **6** (148 mg; 0.27 mmol) was dissolved in 6 M HCl (10 mL) and stirred at 100 °C for 24 hours. Evaporation of the solvent gave H_2**no1th2tha·3HCl** as an off-white solid in quantitative yield (160 mg) (calcd. for 3 HCl, the number of HCl has been determined by potentiometric titration). ^{1}H NMR (D_2O, 300 MHz, 298 K) δ 2.99 (s, 4H, CH_2 tacn), 3.26 (s, 4H, CH_2 tacn), 3.41 (s, 4H, CH_2 tacn), 4.45 (s, 2H, CH_2), 4.54 (s, 4H, CH_2), 7.72 (s, 1H, CH), 7.82 (s, 1H, CH), 8.19 (s, 1H, CH). ^{13}C NMR (D_2O, 75.5 MHz, 298 K) δ 51.1, 53.0, 53.9 (CH_2 tacn), 55.4 (CH_2), 58.3 (CH_2), 127.2 (CH αS), 134.6 (CH αS), 138.6 (CH αN), 148.3 (Cq), 165.7 (C=O), 170.4 (Cq). ESI-HRMS *m*/*z* calcd for $C_{20}H_{25}N_6O_4S_3$, 509.10937; found, 509.10933.

Complex synthesis and characterization

CAUTION! Although no problem arose during our experiments, perchlorate salts and their metal complexes are potentially explosive and should be handled with great care and in small quantities.[40]

General procedure for the complex (1 : 1 M/L ratio) synthesis in water

The ligand (0.1 mmol) was dissolved in 10 mL of water. The pH of the solution was adjusted to *ca.* pH = 6, before the addition of 0.9 equiv. of the corresponding M(II) perchlorate salt. The pH was checked again and stabilized to pH 6.4 to 6.7 by addition of 0.1 M aqueous KOH. The solution was stirred for 12 hours under reflux. After cooling the solution to room temperature, the solvent was evaporated and the residue was collected in MeOH. The desired compound remained insoluble in MeOH while the excess of M(II) perchlorate salts were soluble. The solid was filtered and the process was repeated with MeOH (2 × 3 mL), and then dissolved again in water and dried carefully under reduced pressure.

[Cu(Hno3tha)],·4H_2O. The compound was obtained as a green powder (55 mg, 90%). ESI-HRMS *m*/*z* calcd for $[C_{21}H_{24}N_6O_6S_3Cu]^{2+}$, 307.51022; found, 307.51028.

[Zn(Hno3tha)]. The compound was obtained as a white powder (53 mg, 87%). ^{1}H NMR (D_2O, 300 MHz, 298 K) δ 2.99–3.14 (m, 12H, CH_2 tacn), 4.58 (s, 6H, CH_2), 8.12 (s, 3H, =CH). ESI-HRMS *m*/*z* calcd for $[C_{21}H_{24}N_6O_6S_3Zn]^{2+}$, 308.00999; found, 308.00983.

[Zn(no1th2tha)]. The compound was obtained as a white powder (53 mg, 93%). ^{1}H NMR (D_2O, 400 MHz, 298 K) δ 2.84–2.95 (m, 4H, CH_2 tacn), 2.99–3.02 (m, 2H, CH_2 tacn), 3.11–3.24 (m, 6H, CH_2, tacn), 4.40–4.44 (d, 2H, *J* 16, CH_2), 4.52 (s, 2H, CH_2), 4.54–4.58 (d, 2H, *J* 16, CH_2), 7.28 (d, 1H, *J* 4, =CH) 7.70 (d, 1H, *J* 4, =CH) 8.04 (s, 2H, C=CH). **ESI**-HRMS *m*/*z* calcd for $[C_{20}H_{24}N_6O_4S_3Zn]^{2+}$ 286.0151; found 286.0150.

[Cu(no1th2tha)]. The compound was obtained as a green powder (51 mg, 91%). ESI-HRMS *m*/*z* calcd for $[C_{20}H_{24}N_6O_4S_3Cu]^{2+}$ 285.5153; found 285.5157.

General procedure for the complex (3 : 2 M/L ratio) synthesis in water

The ligand (0.1 mmol) was dissolved in 10 mL of water. The pH of the solution was adjusted to *ca.* pH = 6, before the addition of 1.5 equiv. of the corresponding M(II) perchlorate salt. The pH was checked again and stabilized to pH 6.4 to 6.7 by addition of 0.1 M aqueous KOH. The solution was stirred for 12 hours under reflux. After cooling the solution to room temperature, the solvent was evaporated and the residue was collected in MeOH. The desired compound remained insoluble in MeOH while the excess of M(II) perchlorate salts were soluble. The solid was filtered and the process was repeated with MeOH (2 × 3 mL), and then dissolved again in water and dried under reduced pressure.

Potentiometric studies. The potentiometric setup was described previously.[24] Titrations were performed in aqueous solutions at 0.10 ± 0.01 M of KNO_3 and 25.0 ± 0.1 °C. The titrants were a KOH solution prepared at *ca.* 0.1 M from a commercial ampoule and standardized by application of the Gran method,[41] and also a standard HNO_3 solution at 0.100 M used on back titrations as prepared from a commercial ampoule. A standard solution of ethylenediaminetetraacetic acid dipotassium salt (K_2H_2edta) was prepared at 0.050 M from a commercial ampoule. Ligand (commonly designated as L) solutions were prepared at *ca.* 2.0×10^{-3} M in water acidified with HNO_3 to pH ≈ 2. The Cu^{2+} and Zn^{2+} solutions were prepared at *ca.* 0.05 M from analytical grade nitrate salts and standardized by complexometric titrations[42] with the standard K_2H_2edta solution. Sample solutions for titrations contained approximately 0.03–0.05 mmol of ligand in a 30 mL starting volume, and in complexation titrations metal cations were added at *ca.* 0.9 and 1.5 equiv. of the ligand amount.

The electromotive force during titrations was measured after calibration of the electrode by titration of a standard HNO_3 solution at 2.0×10^{-3} M. The $[H^+]$ of the solutions was determined by measurement of the electromotive force of the cell, $E = E^{\circ\prime} + Q \log [H^+] + E_j$, and the term pH is defined as $-\log [H^+]$. $E^{\circ\prime}$ and Q were determined from the acidic pH region of the calibration titrations. The liquid-junction potential, E_j, was found to be negligible under the experimental conditions used. The value of $K_w = [H^+][OH^-]$ was determined to be equal to $10^{-13.78}$ by titrating a solution of a known hydrogen-ion concentration at the same ionic strength in the alkaline pH region, considering $E^{\circ\prime}$ and Q valid for the entire pH range. The protonation constants of H_4edta and the thermodynamic stability constants of its copper(II) complex used in competition titration refinements were taken from the literature.[43]

Each in-cell titration consisted of *ca.* 120–150 equilibrium points in the range of pH 2.5–11.0, and at least two replicate titrations were performed for each particular system. Back titrations were always performed at the end of each direct complexation titration in order to check if equilibrium was attained throughout the entire pH range. An out-of-cell titration of H_3**no3tha** with copper(II) in the pH range 3.5–5.0 (where equilibrium was not reached during in-cell titrations) was prepared in 10 separate individual points (each at 1/10 the volume of the corresponding analytical solution for the in-cell titration) closed in vials under a nitrogen atmosphere. These points were measured after 4 weeks of stabilization (found by repeated measurement over time of one test vial) and used together with the respective in-cell titration. Competition titrations with H_4edta were also performed for all metal–ligand systems except zinc(II)-H_3**no3tha** to determine the stability constants of the ML complex species, using a 1 : 1 : 1 (Cu/L/edta) ratio at 0.03–0.05

mmol of ligand, such that the competition equilibria taking place are mainly between the ML complex species of edta and of the studied ligands. Thus, only the stability constant for the ML complexes can be accurately obtained from the competition, taking into account that the ML constants for edta are accurately known under our experimental conditions. To determine the full set of stability constants for the various complex species for each metal : ligand system, refinements included the direct titrations performed at both metal ratios (0.9 and 1.5 equiv.) while including the stability constant for the ML species as a fixed value in case it was determined by competition.

The potentiometric data were refined with the HYPERQUAD software,[44] while species distribution diagrams and pM values were calculated using the HySS software.[45] The overall equilibrium constants β^{HL}_{i} and $\beta_{Mm}H_hL_l$ are defined by $\beta^{HL}_{i} = [H_hL_l]/[H]^h[L]^l$ and $\beta_{Mm}H_hL_l = [M_mH_hL_l]/[M]^m[H]^h[L]^l$. Differences, in log units, between the values of protonated (or hydrolysed) and non-protonated constants provide the stepwise (log *K*) reaction constants (being $K_{Mm}H_hL_l = [M_mH_hL_l]/[M_mH_{h-1}L_l][H]$). The errors quoted are the standard deviations calculated by the fitting program for the experimental data in each system.

Spectroscopic studies. Samples of the copper(II) complexes of the macrocyclic ligands were prepared in aqueous solution around neutral pH at *ca.* 1 mM concentration of ligand, using either 0.8–0.9 or 1.5 eq. of Cu^{2+}. These solutions were left for 1–2 days to equilibrate before being used to measure the visible spectra and to prepare the corresponding EPR samples. The visible spectra were acquired on a PerkinElmer lambda 650 spectrophotometer at 25 °C in quartz cuvettes of 1 cm path length. Samples for EPR were prepared from the previous complex solutions by addition of a 5 M $NaClO_4$ solution to 1 M final salt concentration. Samples of the copper(II) complex of H**tha** for EPR were prepared directly using 1 : 2 and 1 : 3 Cu : L ratios in aqueous solutions also at 1 M $NaClO_4$. The EPR spectra of the frozen samples were acquired at 130 K on a Bruker EMX 300 spectrometer operating at the X-band and equipped with a continuous-flow cryostat for liquid nitrogen, at a microwave power of 2.0 mW and a frequency (ν) of 9.51 GHz. The spectra were all simulated using a single paramagnetic species with the SpinCount software.[46]

Electrochemistry. The electrochemical studies were performed in a glovebox (Jacomex) (O_2 < 1 ppm, H_2O < 1 ppm) with a home-designed 3-electrode cell (WE: glassy carbon, RE: Ag/AgCl/NaCl (3 M), CE: graphite rod). The potential of the cell was controlled by using an AUTOLAB PGSTAT 302 (Ecochemie) potentiostat monitored by using a computer. The glassy carbon electrode was carefully polished before each voltammetry experiment with a 1 μm alumina aqueous suspension and ultrasonically rinsed with water and then with acetone. Exhaustive electrolysis was performed with a graphite rod working electrode. The ultrapure (18 MΩ) deoxygenated water was used as received and kept under argon in the glovebox after degassing. Sodium perchlorate (Sigma-Aldrich, 99.99%) was used as a supporting electrolyte in 0.1 M concentration without purification. Experimental redox potential values were recalculated against $E°$ (NHE) by considering that $E°$ (Ag/AgCl/NaCl (3 M)) = 0.22 V *vs.* NHE.

X-ray diffraction studies. X-ray diffraction data were collected with a X-Calibur-2 CCD 4-circle diffractometer (Oxford Diffraction), including a four circle goniometer (KM4) and a two-dimensional CCD detector (SAPPHIRE 2). Three-dimensional X-ray diffraction data were collected on an X-Calibur-2 CCD 4-circle diffractometer (Oxford Diffraction). Data reduction, including interframe scaling, Lorentzian, polarization, empirical absorption, and detector sensitivity corrections, were carried out using programs that are part of CrysAlis software[47] (Oxford Diffraction). Complex scattering factors were determined from the program SHELX97[48] running under the WinGX program system.[49] The structure was solved by direct methods with SIR-97[50] and refined by full-matrix least-squares on F^2. All hydrogen atoms were included in calculated positions and refined in riding mode. Crystal data and details of the data collection and refinement are summarized in Table 6. CCDC numbers 1901777, 1901781 and 1903039 contain the supplementary crystallographic data for this article.

Table 6. Crystal data and structure refinement details for [Cu(H**no3tha**)]·4H_2O (**1**), [Zn(H**no3tha**)] (**2**), [Cu_3(**no3tha**)$_2$](ClO_4)$_2$·6H_2O (**3**), [Cu_3(**no2th1tha**)$_2$](ClO_4)$_4$·2H_2O (**4**), [Cu(**tha**)$_2$] (**5**) and [Cu(**tha**)$_2$]·4H_2O (**6**).

	1	**2**	**3**	**4**	**5**	**6**
Formula	$C_{21}H_{30}N_6O_{10}S_3Cu$	$C_{24}H_{34}Cl_{0.50}N_7O_{11.25}S_3Zn$	$C_{42}H_{54}Cl_2Cu_3N_{12}O_{26}S_6$	$C_{38}H_{50}Cl_4Cu_3N_{12}O_{22}S_6$	$C_8H_4CuN_2O_4S_2$	$C_8H_{12}CuN_2O_8S_2$
MW	686.23	779.86	1596.85	1551.68	319.79	391.86
Crystal syst.	Triclinic	Monoclinic	Monoclinic	Triclinic	Monoclinic	Monoclinic
Space group	$P\bar{1}$	$P2_1/n$	$-P2ybc$	$P\bar{1}$	$P2_1/c$	$P2_1/c$
T/K	296(2)	170(2)	296(2)	296(2)	297(2)	297(2)
λ Å^{-1} (MoK_α)	0.71073	0.71073	0.71073	0.71073	0.71073	0.71073
a/Å	8.9546(4)	9.1563(8)	14.9658(6)	9.7341(6)	5.1905(3)	9.9681(4)
b/Å	10.9939(5)	40.419(3)	13.3025(5)	10.4174(7)	11.6469(7)	7.6471(3)
c/Å	14.0477(6)	17.2257(18)	15.8016(6)	14.3026(8)	8.1551(6)	9.1380(5)
α/°	85.134(4)	90	90	87.718(5)	90	90
β/°	86.799(3)	100.485(10)	103.766(4)	89.646(5)	91.326(7)	96.069(4)
γ/°	81.534(4)	90	90	80.050(5)	90	90
V (Å^3)	1361.62(10)	6268.6(10)	3055.5(2)	1427.39(15)	492.87(5)	692.66(5)
Z	2	8	2	1	2	2
$D_{calc.}$ (g cm^{-3})	1.674	1.653	1.736	1.805	2.155	1.879
μ/mm^{-1}	1.099	1.097	1.419	1.602	2.641	1.918
F(000)	710	3228	1630	789	318	398
θ range (°)	3.72 to 27.468	3.895 to 23.678	3.625 to 24.895	3.41 to 26.37	3.921 to 27.119	4.11 to 28.752
R_{int}	0.1273	0.1771	0.1865	0.153	0.1162	0.0886
Refl. meas.	16 901	29 022	18 817	17 173	1997	4250
Unique refl.	5560	12 795	6226	5817	1008	2047
Refl. obsd	4356	5009	4132	4621	806	1416
GOF on F^2	1.03	0.938	1.035	1.071	1.002	1.061
R_1	0.0468	0.0904	0.0633	0.0558	0.0535	0.0418
wR_2	0.1143	0.1225	0.1621	0.1406	0.1261	0.0827
Largest ≠ peak & hole (e Å^{-3})	0.403–0.508	0.679–0.853	0.861–0.533	0.734–0.685	0.761–0.793	0.413–0.311

DFT studies. Geometry optimisations were carried out employing DFT calculations within the hybrid meta-GGA approximation with the TPSSh exchange–correlation functional[51] and the Gaussian 09 package (Revision E.01).[52] Bulk solvent effects were included by using the integral equation formalism variant of the polarizable continuum model (IEFPCM).[53] The triple-ξ basis set including polarization functions def2-TZVPP proposed by Ahlrichs was used in these calculations.[54] No symmetry constraints have been imposed during the optimisations. The stationary points found on the potential energy surfaces were ensured to represent energy minima rather than saddle points *via* frequency analysis. Gibbs free energies were obtained at T = 298.15 K within the harmonic approximation. The ultrafine integration grid (99 radial shells and 590 angular points) and the default SCF energy convergence criteria (10^{-8}) were used in all calculations.

The calculations of the *g*- and *A*-tensors were carried out using the ORCA program package (version 4.0.1)[55] and the methodology developed by Neese.[56] The *g*-tensor was calculated with the TPSS0 functional,[57] a 25% exchange version of TPSSh (10% exchange) that provides improved energetics.[58] The centre of the electronic charge was taken as the origin for the calculation of the *g*-tensor. The spin–orbit contributions to the hyperfine coupling constants and *g* values were computed *via* the spin–orbit mean field approach (SOMF) using the one-centre approximation to the exchange term (SOMF(1X)).[59] The basis set used for the calculation of EPR parameters comprised the aug-cc-pVTZ-J basis set of Sauer for Cu,[60] and Ahlrichs' def2-TZVPP basis set for all other atoms. The RIJCOSX approximation[61] was used to speed up the

calculations of the EPR parameters using the auxiliary basis sets constructed automatically by ORCA with the *autoaux* keyword.[62] The convergence tolerances and integration accuracies of the calculations were increased from the defaults using the available TightSCF and Grid5 options (Grid7 for Cu). Solvent effects (water) were taken into account by using the SMD solvation model.[63]

Conflicts of interest

The authors declare no conflict of interest.

Acknowledgements

R. T. and V. P. acknowledge the Ministère de l′Enseignement Supérieur et de la Recherche, the Centre National de la Recherche Scientifique and the "Service Commun" of NMR facilities of the University of Brest. R.D. and L.M.P.L. acknowledge Fundação para a Ciência e a Tecnologia (FCT) for the financial support under Project LISBOA-01-0145-FEDER-007660 (Microbiologia Molecular, Estrutural e Celular) funded by FEDER funds through COMPETE2020 – Programa Operacional Competitividade e Internacionalização (POCI) and by national funds through FCT, and L. M. P. L. thanks FCT also for a postdoctoral fellowship (SFRH/BPD/73361/2010). C. P.-I. and D. E.-G. thank Centro de Computación de Galicia (CESGA) for providing the computer facilities.

References

01 (*a*) E. Atrián-Blasco, P. Gonzalez, A. Santoro, B. Alies, P. Faller and C. Hureau, *Coord. Chem. Rev.*, 2018, **371**, 38–55; (*b*) E. Atrián-Blasco, A. Santoro, D. L. Pountney, G. Meloni, C. Hureau and P. Faller, *Chem. Soc. Rev.*, 2017, **46**, 7683–7693; (*c*) E. Atrián-Blasco, A. Conte-Daban and C. Hureau, *Dalton Trans.*, 2017, **46**, 12750–12759.

02 (*a*) E. Salvadeo, L. Dubois and J.-M. Latour, *Coord. Chem. Rev.*, 2018, **374**, 345–375; (*b*) S. Wherland, O. Farver and I. Pecht, *J. Inorg. Biochem.*, 2014, **19**, 541–554; (*c*) E. Solomon, A. J. Augustine and J. Yoon, *Dalton Trans.*, 2008, 3921–3932.

03 D. Denoyer, S. A. S. Sharnel and M. A. Cater, Copper Complexes in Cancer Therapy, in *Metallo-Drugs: Development and Action of Anticancer Agents*, eds. A. Sigel, H. Sigel, E. Freisinger and R. K. O. Sigel, Walter de Gruyter GmbH, Berlin, 2018.

04 (*a*) E. Boros and A. B. Packard, *Chem. Rev.*, 2019, **119**, 870–901; (*b*) E. W. Price and C. Orvig, *Chem. Soc. Rev.*, 2014, **43**, 260–290; (*c*) R. Chakravarty, S. Chakraborty and A. Dash, *Mol. Pharmaceutics*, 2016, **13**, 3601–3612; (*d*) C. L. Charron, A. L. Farnsworth, P. D. Roselt, R. J. Hicks and C. A. Hutton, *Tetrahedron Lett.*, 2016, **57**, 4119–4127.

05 R. G. Pearson, *J. Am. Chem. Soc.*, 1963, **85**, 3533–3539.

06 (*a*) T. J. P. McGivern, S. Afsharpour and C. J. Marmion, *Inorg. Chim. Acta*, 2018, **472**, 12–39; (*b*) X. Liu, C. Manzur, N. Novoa, S. Celedón, T. Carrillo and J.-R. Hamon, *Coord. Chem. Rev.*, 2018, **357**, 144–172; (*c*) A. Erxleben, *Coord. Chem. Rev.*, 2018, **360**, 92–121.

07 (*a*) I. Lukes, J. Kotek, P. Vojtísek and P. Hermann, *Coord. Chem. Rev.*, 2001, **216–217**, 287–312; (*b*) C. J. Anderson and R. Ferdani, *Cancer Biother. Radiopharm.*, 2009, **24**, 379–393.

08 K. S. Woodin, K. J. Heroux, C. A. Boswell, E. H. Wong, G. R. Weisman, W. Niu, S. A. Tomellini, C. J. Anderson, L. N. Zakharov and A. L. Rheingold, *Eur. J. Inorg. Chem.*, 2005, 4829–4833.

09 (*a*) A. Bevilaqua, R. I. Gelb, W. B. Hebard and L. J. Zompa, *Inorg. Chem.*, 1987, **26**, 2699; (*b*) K. Wieghardt, U. Bossek, P. Chaudhuri, W. Herrmann, B. C. Menke and J. Weiss, *Inorg. Chem.*, 1982, **21**, 4308–4313; (*c*) V. Maheshwari, J. L. J. Dearling, S. T. Treves and A. B. Packard, *Inorg. Chim. Acta*, 2012, **393**, 318–323; (*d*) A. C. Warden, L. Spiccia, M. T. W. Hearn, J. F. Boas and J. R. Pilbrow, *Dalton Trans.*, 2005, 1804–1813; (*e*) J. Qian, L.-P. Wang, J.-L. Tian, C.-Z. Xie and S.-P. Yan, *J. Coord. Chem.*, 2012, **65**, 122–130.

10 (*a*) W. Han, Z.-D. Wang, C.-Z. Xie, Z.-Q. Liu, S.-P. Yan, D.-Z. Liao, Z.-H. Jiang and P. Cheng, *J. Chem. Crystallogr.*, 2004, **34**, 495–500; (*b*) M. Roger, V. Patinec, R. Tripier, S. Triki, N. Le Poul and Y. Le Mest, *Inorg. Chim. Acta*, 2014, **417**, 201–207; (*c*) S. J. Brudenell, L. Spiccia, A. M. Bond, P. Comba and D. C. R. Hockless, *Inorg. Chem.*, 1998, **37**, 3705–3713; (*d*) T. C. Pickel, G. J. Karahalis, C. T. Buru, J. Bacsa and C. C. Scarborough, *Eur. J. Org. Chem.*, 2018, 6876–6889.

11 C. Gotzmann, F. Braun and M. D. Bartolomä, *RSC Adv.*, 2016, **6**, 119–131.

12 (*a*) D. Schulz, T. Weyhermüller, K. Wieghardt, C. Butzlaff and A. X. Trautwein, *Inorg. Chim. Acta*, 1996, **246**, 387–394; (*b*) U. Auerbach, U. Eckert, K. Wieghardt, B. Nuber and J. Weiss, *Inorg. Chem.*, 1990, **29**, 938–944; (*c*) V. R. de Almeida, F. R. Xavier, R. E. H. M. B. Osório, L. M. Bessa, E. L. Schilling, T. G. Costa, T. Bortolotto, A. Cavalett, F. A. V. Castro, F. Vilhena, O. C. Alves, H. Terenzi, E. C. A. Eleutherio, M. D. Pereira, W. Haase, Z. Tomkowicz, B. Szpoganicz, A. J. Bortoluzzi and A. Neves, *Dalton Trans.*, 2013, **42**, 7059–7073; (*d*) E. Arturoni, C. Bazzicalupi, A. Bencini, C. Caltagirone, A. Danesi, A. Garau, C. Giorgi, V. Lippolis and B. Valtancoli, *Inorg. Chem.*, 2008, **47**, 6551–6563.

13 (*a*) A. Guillou, L. M. P. Lima, M. Roger, D. Esteban-Gómez, R. Delgado, C. Platas-Iglesias, V. Patinec and R. Tripier, *Eur. J. Inorg. Chem.*, 2017, 2435–2443; (*b*) M. Roger, L. M. P. Lima, M. Frindel, C. Platas-Iglesias, J.-F. Gestin, R. Delgado, V. Patinec and R. Tripier, *Inorg. Chem.*, 2013, **52**, 5246–5259.

14 T. Joshi, B. Graham and L. Spiccia, *Acc. Chem. Res.*, 2015, **48**, 2366–2379.

15 (*a*) P. Chaudhuri, I. Karpestein, M. Winter, M. Lengen, C. Butzlaff, E. Bill, A. X. Trautwein, U. Flörke and H.-J. Haupt, *Inorg. Chem.*, 1993, **32**, 888–894; (*b*) D. J. Elliot, L. L. Martin and M. R. Taylor, *Acta Crystallogr., Sect. C: Cryst. Struct. Commun.*, 1998, **54**, 1259–1261; (*c*) F. H. Fry, P. Jensen, C. M. Kepert and L. Spiccia, *Inorg. Chem.*, 2003, **42**, 5637–5644; (*d*) J. W. Steed, A. E. Goeta, J. Lipkowski, D. Swierczynski, V. Panteleon and S. Handa, *Chem. Commun.*, 2007, 813–815.

16 (*a*) M. Raidt, M. Neuburger and T. A. Kaden, *Dalton Trans.*, 2003, 1292–1298.

17 D. Montagner, V. Gandin, C. Marzan and A. Erxleben, *J. Inorg. Biochem.*, 2015, **145**, 101–107.

18 M. J. Belousoff, B. Graham and L. Spiccia, *Eur. J. Inorg. Chem.*, 2008, 4133–4139.

19 R. Cao, P. Müller and S. J. Lippard, *J. Am. Chem. Soc.*, 2010, **132**, 17366–17369.

20 (*a*) C. J. Coghlan, E. M. Campi, S. R. Batten, W. R. Jackson and M. T. W. Hearn, *Polyhedron*, 2016, **105**, 246–252; (*b*) C. J. Coghlan, E. M. Campi, C. M. Forsyth, W. R. Jackson and M. T. W. Hearn, *Aust. J. Chem.*, 2015, **68**, 1115–1121.

21 L. Tang, J. Park, H.-J. Kim, Y. Kim, S. J. Kim, J. Chin and K. M. Kim, *J. Am. Chem. Soc.*, 2008, **130**, 12606–12607.

22 L. Nagel, C. M. Forsyth and L. L. Martin, *Acta Crystallogr., Sect. E: Struct. Rep. Online*, 2007, **63**, m2193.

23 M. Le Fur, M. Beyler, N. Le Poul, L. M. P. Lima, Y. Le Mest, R. Delgado, C. Platas-Iglesias, V. Patinec and R. Tripier, *Dalton Trans.*, 2016, **45**, 7406–7420.

24 A. Guillou, L. M. P. Lima, D. Esteban-Gómez, N. Le Poul, M. D. Bartholomä, C. Platas-Iglesias, R. Delgado, V. Patinec and R. Tripier, *Inorg. Chem.*, 2019, **58**, 2669–2685.

25 (*a*) T. J. Atkins, *J. Am. Chem. Soc.*, 1980, **102**, 6365–6369; (*b*) G. R. Weisman, D. J. Vachon, V. B. Johnson and D. A. Gronbeck, *J. Chem. Soc., Chem. Commun.*, 1987, 886–887.

26 M. J. Van der Merve, J. C. A. Boeyens and R. D. Hancock, *Inorg. Chem.*, 1985, **24**, 1208–1213.

27 C. F. G. C. Geraldes, M. C. Alpoim, M. P. M. Marques, A. D. Sherry and M. Singh, *Inorg. Chem.*, 1985, **24**, 3876–3881.

28 W. R. Harris, C. J. Carrano and K. N. Raymond, *J. Am. Chem. Soc.*, 1979, **101**, 2213–2214.

29 (*a*) P. Torres-García, F. Luna-Giles, Á. Bernalte-García, C. Platas-Iglesias, D. Esteban-Gómez and E. Viñuelas-Zahínos, *New J. Chem.*, 2017, **41**, 8818–8827; (*b*) A. Carné-Sánchez, C. S. Bonnet, I. Imaz, J. Lorenzo, E. Tóth and D. Maspoch, *J. Am. Chem. Soc.*, 2013, **135**, 17711–17714; (*c*) Y. Habata, M. Ikeda, A. K. Sah, K. Noto and S. Kuwahara, *Inorg. Chem.*, 2013, **52**, 11697–11699; (*d*) C. V. Esteves, J. Madureira, L. M. P. Lima, P. Mateus, I. Bento and R. Delgado, *Inorg. Chem.*, 2014, **53**, 4371–4386.

30 (*a*) N. Camus, Z. Halime, N. Le Bris, H. Bernard, C. Platas-Iglesias and R. Tripier, *J. Org. Chem.*, 2014, **79**, 1885; (*b*) T.-H. Lu, S.-C. Lin, H. Aneetha, K. Panneerselvam and C.-S. Chung, *J. Chem. Soc., Dalton Trans.*, 1999, 3385–3391.

31 (*a*) N. Meundaeng, A. Rujiwatra and T. J. Prior, *Transition Met. Chem.*, 2016, **41**, 783–793; (*b*) A. Rossin, B. Di Credico, G. Giambastiani, L. Gonzalvi, M. Peruzzini and G. Reginato, *Eur. J. Inorg. Chem.*, 2011, 539–548.

32 C. L. Klein, R. J. Majeste, L. M. Trefonas and C. J. O'Connor, *Inorg. Chem.*, 1982, **21**, 1891–1897.

33 C.-L. Chen, J. M. Ellsworth, A. M. Goforth, M. D. Smith, C.-Y. Su and H.-C. zur Loye, *Dalton Trans.*, 2006, 5278–5286.

34 M. Trivedi, D. S. Pandey and N. P. Rath, *Acta Crystallogr., Sect. E: Struct. Rep. Online*, 2009, **63**, m303.

35 (*a*) K.-Y. Choi, Y.-M. Jeon, H. Ryu, J.-J. Oh, H.-H. Lim and M.-W. Kim, *Polyhedron*, 2004, **23**, 903–911; (*b*) I. Carreira-Barral, M. Mato-Iglesias, A. de Blas, C. Platas-Iglesias, P. A. Tasker and D. Esteban-Gómez, *Dalton Trans.*, 2017, **46**, 3192–3206.

36 Z. Hua-Ming, W. Shao-Yi, K. Min-Quan and Z. Zhi-Hong, *J. Phys. Chem. Solids*, 2012, **73**, 846–850.

37 (*a*) D. Kivelson and R. Neiman, *J. Chem. Phys.*, 1961, **35**, 149; (*b*) M. Labanowska, E. Bidzinska, A. Para and M. Kurdziel, *Carbohydr. Polym.*, 2012, **87**, 2605–2613.

38 H. Meier, F. Nicklas and R. Z. Petermann, *Z. Naturforsch.*, 2007, **62b**, 1525.

39 A. Aditya and T. Kodadek, *ACS Comb. Sci.*, 2012, **14**, 164–169.

40 W. C. Wolsey, *J. Chem. Educ.*, 1973, **50**, A335.

41 F. J. C. Rossotti and H. Rossotti, *J. Chem. Educ.*, 1965, **42**, 375–378.

42 G. Schwarzenbach and W. Flaschka, *Complexometric Titrations*, Methuen & Co, London, 1969.

43 L. D. Pettit and H. K. J. Powell, IUPAC Stability Constants Database, version 5.85, Academic Software, Timble, 2005.

44 P. Gans, A. Sabatini and A. Vacca, *Talanta*, 1996, **43**, 1739–1753.

45 L. Alderighi, P. Gans, A. Ienco, D. Peters, A. Sabatini and A. Vacca, *Coord. Chem. Rev.*, 1999, **184**, 311–318.

46 D. Petasis and M. Hendrich, *Methods Enzymol.*, 2015, **563**, 171–208.

47 (*a*) *CrysAlis CCD, version 1.171.33.52*, Oxford Diffraction Ltd., Oxfordshire, UK, 2009; (*b*) *CrysAlis RED, version 1.171.33.52*, Oxford Diffraction Ltd., Oxfordshire, UK, 2009.

48 G. M. Sheldrick, *Acta Crystallogr., Sect. A: Found. Crystallogr.*, 2008, **64**, 112–122.

49 L. J. Farrugia, *J. Appl. Crystallogr.*, 1999, **32**, 837–838.

50 A. Altomare, M. C. Burla, M. Camalli, G. L. Cascarano, C. Giacovazzo, A. Guagliardi, A. G. G. Moliterni, G. Polidori and R. Spagna, *J. Appl. Crystallogr.*, 1999, **32**, 115–119.

51 J. M. Tao, J. P. Perdew, V. N. Staroverov and G. E. Scuseria, *Phys. Rev. Lett.*, 2003, **91**, 146401.

52 M. J. Frisch, G. W. Trucks, H. B. Schlegel, G. E. Scuseria, M. A. Robb, J. R. Cheeseman, G. Scalmani, V. Barone, B. Mennucci, G. A. Petersson, H. Nakatsuji, M. Caricato, X. Li, H. P. Hratchian, A. F. Izmaylov, J. Bloino, G. Zheng, J. L. Sonnenberg, M. Hada, M. Ehara, K. Toyota, R. Fukuda, J. Hasegawa, M. Ishida, T. Nakajima, Y. Honda, O. Kitao, H. Nakai, T. Vreven, Jr., J. A. Montgomery, J. E. Peralta, F. Ogliaro, M. Bearpark, J. J. Heyd, E. Brothers, K. N. Kudin, V. N. Staroverov, R. Kobayashi, J. Normand, K. Raghavachari, A. Rendell, J. C. Burant, S. S. Iyengar, J. Tomasi, M. Cossi, N. Rega, N. J. Millam, M. Klene, J. E. Knox, J. B. Cross, V. Bakken, C. Adamo, J. Jaramillo, R. Gomperts, R. E. Stratmann, O. Yazyev, A. J. Austin, R. Cammi, C. Pomelli, J. W. Ochterski, R. L. Martin, K. Morokuma, V. G. Zakrzewski, G. A. Voth, P. Salvador, J. J. Dannenberg, S. Dapprich, A. D. Daniels, Ö. Farkas, J. B. Foresman, J. V. Ortiz, J. Cioslowski and D. J. Fox, *Gaussian 09, Revision E.01*, Gaussian, Inc., Wallingford CT, 2009.

53 J. Tomasi, B. Mennucci and R. Cammi, *Chem. Rev.*, 2005, **105**, 2999–3093.

54 F. Weigend and R. Ahlrichs, *Phys. Chem. Chem. Phys.*, 2005, **7**, 3297.

55 F. Neese, *Wiley Interdiscip. Rev.: Comput. Mol. Sci.*, 2012, **2**, 73–78.

56 (*a*) F. Neese, *J. Chem. Phys.*, 2003, **117**, 3939; (*b*) F. Neese, *J. Chem. Phys.*, 2001, **115**, 11080; (*c*) F. Neese, *J. Phys. Chem. A*, 2001, **105**, 4290–4299.

57 S. Grimme, *J. Phys. Chem. A*, 2005, **109**, 3067–3077.

58 (*a*) M. K. Kesharwani and J. M. L. Martin, *Theor. Chem. Acc.*, 2014, **133**, 1452; (*b*) A. Marzouk, B. Madebène and M. E. Alikhani, *J. Phys. Chem. A*, 2013, **117**, 4462–4471.

59 F. Neese, *J. Chem. Phys.*, 2005, **122**, 034107.

60 (*a*) E. D. Hedegard, J. Kongsted and S. P. A. Sauer, *J. Chem. Theory Comput.*, 2011, **7**, 4077–4087; (*b*) F. Neese, F. Wennmohs, A. Hansen and U. Becker, *Chem. Phys.*, 2009, **356**, 98–109; (*c*) R. Izsak and F. Neese, *J. Chem. Phys.*, 2011, **135**, 144105; (*d*) T. Petrenko, S. Kossmann and F. Neese, *J. Chem. Phys.*, 2011, **134**, 054116.

61 S. Kossmann and F. Neese, *Chem. Phys. Lett.*, 2009, **481**, 240–243.

62 G. L. Stoychev, A. A. Auer and F. Neese, *J. Chem. Theory Comput.*, 2017, **13**, 554–562.

63 A. V. Marenich, C. J. Cramer and D. G. Truhlar, *J. Phys. Chem. B*, 2009, **113**, 6378–6396.

[i] Electronic supplementary information (ESI) available: NMR and MS, overall equilibrium constants, species distribution diagrams, additional EPR data and DFT optimised geometries and Cartesian coordinates. CCDC 1901777, 1901781 and 1903039. For ESI and crystallographic data in CIF or other electronic format see DOI: 10.1039/c9dt01366k.